JGR Oceans

RESEARCH ARTICLE
10.1029/2023JC020453

Expanded Understanding of the Western Antarctic Peninsula Sea-Ice Environment Through Local and Regional Observations at Palmer Station

E. Goodell[1], S. Stammerjohn[2], M. Meredith[3], C. Moffat[4], and R. Eveleth[1]

[1]Department of Geosciences, Oberlin College, Oberlin, OH, USA, [2]Institute of Arctic and Alpine Research, University of Colorado Boulder, Boulder, CO, USA, [3]British Antarctic Survey, Cambridge, UK, [4]School of Marine Science & Policy, University of Delaware, Newark, DE, USA

Key Points:

- Local-scale sea-ice measurements at Palmer Station show higher daily and interannual variability than satellite-based measurements
- Northwestward winter ice movement typically preceded elevated spring sea-ice meltwater near Palmer Station
- Local sea-ice retreat influences water column stratification and Chlorophyll-*a* but does not explain increasing trends in these parameters

Supporting Information:

Supporting Information may be found in the online version of this article.

Correspondence to:

R. Eveleth,
reveleth@oberlin.edu

Citation:

Goodell, E., Stammerjohn, S., Meredith, M., Moffat, C., & Eveleth, R. (2024). Expanded understanding of the Western Antarctic Peninsula sea-ice environment through local and regional observations at Palmer Station. *Journal of Geophysical Research: Oceans*, *129*, e2023JC020453. https://doi.org/10.1029/2023JC020453

Received 6 SEP 2023
Accepted 19 OCT 2024

Author Contributions:

Conceptualization: R. Eveleth
Data curation: M. Meredith, C. Moffat
Formal analysis: E. Goodell, S. Stammerjohn, R. Eveleth
Funding acquisition: M. Meredith, C. Moffat, R. Eveleth
Investigation: E. Goodell
Methodology: E. Goodell, R. Eveleth
Project administration: R. Eveleth
Resources: S. Stammerjohn
Supervision: R. Eveleth
Validation: R. Eveleth
Visualization: E. Goodell
Writing – original draft: E. Goodell
Writing – review & editing: E. Goodell, S. Stammerjohn, M. Meredith, C. Moffat, R. Eveleth

Abstract The Western Antarctic Peninsula (WAP) has been experiencing rapid regional warming since at least the 1950s, however, the impacts of this warming at the local scale are variable and nuanced. Previous studies that have linked sea-ice variability to biogeochemical cycles and food web dynamics often combine local-scale biogeochemical data with coarse-resolution regional satellite sea-ice data, which may not adequately capture local sea-ice conditions. In this study, we analyzed local-scale in situ sea-ice observations collected as part of a 28-year record (1992–2020) from the Palmer Long-Term Ecological Research site at Anvers Island, mid-WAP, in conjunction with isotopically-derived sea-ice meltwater (SIM) fractions and satellite-derived sea-ice motion and concentration, to quantify the variability and long-term trends in local sea-ice behavior. In situ sea ice observations at Palmer Station displayed higher variability than satellite observations and showed no significant declines over this time, despite region-wide declines identified in prior studies. Higher spring SIM fractions were attributed to strong northward sea-ice motion throughout the winter. Applying these local-scale sea-ice insights to similarly scaled stratification and chlorophyll-*a* measurements, we found that a longer-lasting, more consistent sea-ice pack led to greater water column stratification following the spring sea-ice retreat. Greater sea-ice persistence and stronger stratification led to larger peaks in chlorophyll-*a*, though sea-ice metrics did not explain the positive temporal trends in either stratification strength or chlorophyll-*a*. Through this study, we identify how local sea-ice observations and meltwater data can enhance satellite data to build an understanding of the intricate connections between ice, water column dynamics, and phytoplankton.

Plain Language Summary The western coast of the Antarctic Peninsula is one of the fastest-warming places on the planet. The coastal ocean here is home to large amounts of marine algae (phytoplankton), which supports a rich ecosystem. Prior studies have noted that sea ice plays a role in determining how abundant phytoplankton are in the water, but these studies typically use sea-ice measurements from regional-scale satellites, which do not always provide details about how sea ice is behaving at the local scale. Here, we analyze a daily sea-ice record that was acquired locally through visual observation, as well as local-scale ocean water samples that detect how much sea-ice meltwater is present. We found that, despite regional warming, high year-to-year variability masks long-term trends in the local sea-ice record, and that the movement of sea ice during winter influences how much sea ice melts in place when it retreats in the spring. We also found that years with greater winter sea-ice coverage led to summers with more ideal conditions for phytoplankton growth (e.g., shallower and more stratified water), though sea ice does not appear to be the primary driver behind recent increases in phytoplankton.

1. Introduction

Sea ice around the continent of Antarctica plays an important role in the coastal marine ecosystem, as well as in the magnitude and variability of the Southern Ocean carbon sink (Death et al., 2014; Rintoul, 2018). The Southern Ocean hosts spatially variable and predominantly seasonal sea ice, with very little surviving through each summer to become multi-year ice. Unlike the Arctic Ocean, where sea ice has substantially declined since the 1980s in response to anthropogenic warming (Meier et al., 2014; Parkinson et al., 1999), sea-ice trends in the Southern Ocean are highly variable, both regionally and seasonally, with opposing regional trends (Holland & Kwok, 2012; Massom et al., 2013) contributing to an overall weak Antarctic-wide positive sea-ice trend (Comiso & Nishio, 2008; Turner et al., 2014). The Amundsen and Bellingshausen Seas for example, saw strong negative

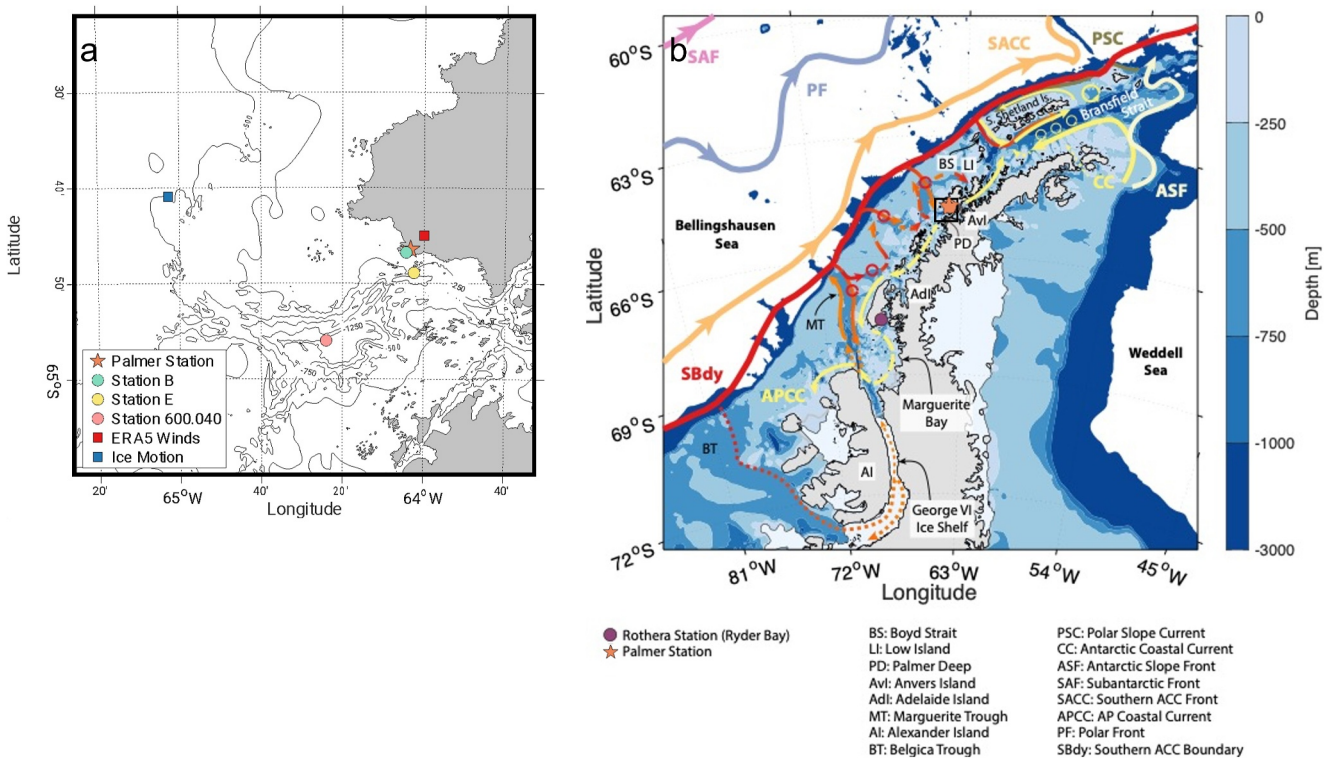

Figure 1. Maps of study location at the Antarctic Peninsula. (a) Close-up of bathymetry offshore of Anvers Island showing relevant locations referenced in this study (Palmer Station where in situ ice observations were made, LTER grid site 600.040 the grid cell of matched satellite ice observations, Stations B and E, the ERA5 wind site, and the center of the ice motion grid cell closest to Palmer). (b) A map of bathymetry, major currents and ice shelves along the Antarctic Peninsula, modified from Moffat and Meredith (2018). The black box indicates the location shown in panel (a).

sea-ice trends between 1979 and 2015, while the Ross and Weddell Seas exhibited strong positive trends (Maksym, 2019; Parkinson, 2019; Turner et al., 2022), emphasizing the importance of regionally-resolved sea-ice studies (Stroeve et al., 2016). Further, in recent years Antarctic sea ice exhibited dramatic swings from record highs in 2012–2014 to record low years since 2016 (Liu et al., 2023; Meehl et al., 2019; Parkinson, 2019; Turner et al., 2022) and has increased in variance since 2022 (Hobbs et al., 2024), such that Antarctic-wide sea-ice extent trends are no longer significant (Maksym, 2019).

The Western Antarctic Peninsula (WAP), which stretches to the northernmost latitudes of Antarctica (Figures 1a–1b) warmed an estimated 6–7° in winter months from 1951 to 2001 (Vaughan et al., 2003), significantly faster than other regions of Antarctica (Turner et al., 2005, 2014). In recent years, high interannual variability, likely caused by natural climate oscillations, has complicated the identification of atmospheric warming trends (Turner et al., 2016), however, this variability does not negate the presence of decadal trends and their likely persistence into the future (Stammerjohn & Scambos, 2020; Turner et al., 2016). Continued warming of the WAP has implications for both coastal marine and terrestrial processes. Warmer shelf ocean temperatures are causing thinning and accelerated breakup of marine-terminating glaciers (Rignot et al., 2019; Wouters et al., 2015), accelerating glacial retreat and contributing to sea level rise (Cook et al., 2005). Accelerated continental ice loss also has the potential to influence coastal biogeochemistry through the delivery of essential micro-nutrients (e.g., iron) and the modulation of coastal stratification and mixing rates in the upper ocean (Cape et al., 2019; Hopwood et al., 2019; Smith et al., 2011).

Since systematic satellite observations began in late 1978, sea-ice extent has declined across the WAP region. The decline was characterized by delayed autumnal freeze-up and earlier spring retreat (Stammerjohn, Martinson, Smith, Yuan, & Rind, 2008), most pronounced through 2010, followed by several years of greater WAP sea-ice coverage (Schofield et al., 2018). Studies have attributed spatial and temporal sea-ice variability to regional climate oscillations, such as the Southern Annular Mode and El Niño-Southern Oscillation (Hobbs et al., 2016; Kwok et al., 2016; Stammerjohn, Martinson, Smith, Yuan, & Rind, 2008), and intra-seasonal wind patterns (Baba

et al., 2006; Kimura, 2007). Stammerjohn and Scambos (2020) summarize how our understanding of long-term trends in Antarctic sea ice, including along the WAP, is complicated by the presence of short-term climate variations which oscillate between masking and amplifying long-term trends.

Changes in sea-ice behavior and extent impact water column characteristics, biogeochemical cycles, and the marine ecosystem by altering light availability, wind influence, air-sea interactions, and fluxes of brine/freshwater, nutrients, or potentially ice algae to the water column. Historically sea ice dynamics and their implications along the WAP have been investigated using coarse-resolution (25 km) satellite (SSM/I-SSMIS)-derived ice metrics. This data set is the source of the only long-term satellite time series (1979–2024) near Palmer Station and has greatly aided the study of climate change.

Using SSM/I-SSMIS ice metrics, studies have concluded that greater sea-ice cover leads to shallower mixed layer depths and increased summer chl-*a*, and typically attribute this connection to sea-ice presence leading to an influx of buoyant, stratifying meltwater during spring retreat (Carvalho et al., 2016; Saba et al., 2014; Schofield et al., 2018; Vernet et al., 2008). Montes-Hugo et al. (2009) found decreasing chl-*a* trends in the northern WAP region, which they attributed to declines in sea-ice extent, while in the southern region declines in sea-ice extent caused increases in chl-*a*. This north-south discrepancy was due to the fact these WAP-wide sea-ice decreases were superimposed on a north-south gradient of short versus long sea-ice seasons, such that decreased sea ice in the south led to an earlier relief from light limitation from a too persistent sea ice cover (whereas decreased sea ice in the north led to increased wind mixing facilitated by a now greatly shortened ice season). Turner et al. (2024) found that spring bloom timing along the sea-ice associated region of the WAP has moved later into the spring, a change they attribute to increased spring wind speed.

Many of the studies utilizing satellite sea-ice data focused on the rapid decline in sea-ice extent and duration along the WAP that was observed between 1979 and 2008. More recently Schofield et al. (2018) reported that this sea-ice decline reversed between 2008 and 2015, and they found that in response to the increase in sea-ice extent, there was a consequent shoaling of the mixed layer in the southern WAP region (not including Palmer Station), which in turn caused an increase in primary production. This study is among several that have identified how interactions between sea ice, the water column, and biogeochemistry vary across the WAP and demonstrate the importance of identifying locally relevant mechanisms (Kim et al., 2018; Montes-Hugo et al., 2009).

Ice concentration and type is much more spatially variable on local scales than can be resolved in the SSM/I-SSMIS record, an example of which can be seen in the 0.48 m resolution WorldView 2 image of Palmer Station in Figure 2b. While satellites such as WorldView 2 have been helpful for recording high spatial variability in ice cover and type, and helping validate concentration observations (Figure 2), cloud-free images are too sparse to be used for time series analysis. Thus, field observations provide a critical opportunity to investigate local sea-ice dynamics and their implications, as demonstrated at Rothera Research Station to the south of Palmer (Biggs et al., 2019; Venables et al., 2013, 2023).

The Palmer Station Long-Term Ecological Research (Pal-LTER) program, based midway along the WAP on Anvers Island (Figure 1b), has collected physical, chemical, and biological data since 1991. Its latitudinal position along the peninsula provides the opportunity to investigate the properties of the transition zone between the northern and southern sub-regions (e.g., Montes-Hugo et al., 2009). In this study, we analyze Pal-LTER data, including previously unpublished in situ sea-ice observations and an expanded analysis of the oxygen isotope freshwater record, in conjunction with more commonly used regional satellite sea-ice observations to quantify if and how sea ice continues to change near Palmer Station, and to investigate how local (in situ) and regional (satellite) sea-ice data can provide insights into the complex ways sea-ice shapes the coastal marine environment.

2. Methods

2.1. Sea Ice

In situ sea-ice data were collected from 1992 to 2020 as part of the Pal-LTER program. Data are unavailable for the 2020–2021 and 2021-2022 sea-ice seasons due to COVID-19 and on-station construction. Observations were made daily by an on-station technician visually estimating sea-ice concentration and type (i.e., frazil, pancake, brash, and fast) following a standardized protocol using World Meteorological Organization coding (World Meteorological Organization (2017)). While these sea-ice measurements are subjective and potentially prone to

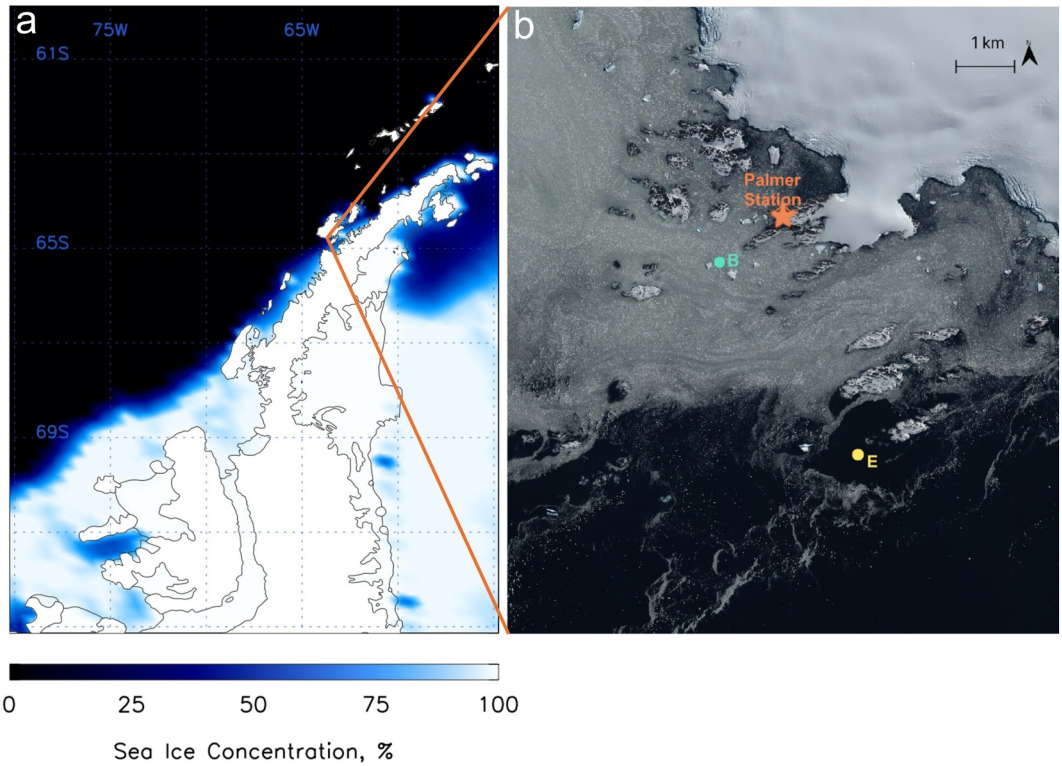

Figure 2. Satellite observations of ice near Palmer Station on 16 December 2016. (a) Coarse-resolution (25 km) passive microwave satellite-derive ice concentration from SSM/I-SSMIS with a concentration of 35% at the closest LTER grid site to Palmer on the day of the image. (b) Very high-resolution (<0.5 m) optical satellite image from WorldView 2 (copyright 2016 Maxar) with Palmer Station marked in orange, Station B in turquoise (1 km from Palmer), and Station E in yellow (5 km from Palmer). The visually observed concentration from Palmer Station on that day was 75%. The average visibility at Palmer Station is 31 km.

observer biases, they provide a daily time series of sea-ice behavior directly at our location of interest and remain the only available source that regularly records sea-ice type.

Sea-ice concentrations were reported using a 0–9 code, where each code represents a bin of concentration values or description of the distribution of sea ice (Table 1). The midpoint of each concentration bin was used where numerical values were provided (codes 0 and 2–5). Instances that could be reasonably matched to a concentration (codes 6, 7, 9) were included in analyses. Code 9, though somewhat ambiguous, was estimated at 75% ice cover which likely represents a lower bound on this ice concentration bin. Additionally, code 9 was used in less than 2% of records, and mapping code 9 onto a concentration of 90% or 75% does not change any of the calculated annual sea-ice metrics. Several sea-ice codes do not translate clearly to a percent coverage estimate. Instances where a code had no clear concentration equivalent (codes 1 and 8) were not included. Eliminating these codes did not impact annual sea-ice metrics and further analyses, with the exception of sea-ice year 1995–1996, when code 8 was used with anomalously high frequency. The ambiguity of code 8 makes it challenging to confidently estimate a concentration equivalent. Because of this, satellite-derived annual sea-ice metrics were used in place of in situ metrics during this year, and the year was consequently omitted in analyses comparing satellite and in situ sea-ice records. One limitation of the in situ sea-ice record is the structure of binning of sea-ice concentration data into unequal and large bins. The largest bin encompasses sea-ice concentrations between 15% and 50%, making detailed analyses of daily sea-ice behavior challenging. Sea-ice type is also reported using a code system, with values corresponding to specific sea-ice types of increasing age and thickness (Table 1).

We compare field ice observations to satellite-derived ice concentrations from Scanning Multi-channel Microwave Radiometer-Special Sensor Microwave/Imager, gridded to 25 km (Figure 2a). We utilized satellite data from the Pal-LTER grid location 600.040 (Figure 1a). This site, despite being 23 km from Palmer Station, has

Table 1
World Meteorological Organization Ice Concentration Code, Description, and Our Equivalent Percent Coverage (Sea-Ice Type Codes and Descriptions Follow)

Ice code	Description	Concentration equivalent (%)
0	No ice in sight	0
1	Ship in open lead >1 nm wide, or ship in fast ice with boundary beyond limit of visibility	Not used
2	Sea ice present <3/10, lots of open water	15
3	4/10–16/10 open pack ice	50
4	7/10–18/10 close pack ice	75
5	9/10 or more, but not 10/10, very close pack	95
6	Strips and patches of pack with open water between	10
7	Strips or patches of close or very close pack ice with areas of lower concentration between	50
8	Fast ice with open water, very open or open pack ice to seaward of the ice boundary.	Not used
9	Fast ice with close or very close pack ice to sea of ice boundary	75
Ice Type Code	**Description**	
0	New ice only (Frazil ice, grease ice, slush, shuga)	–
1	Nilas or ice rind, less than 10 cm thick	–
2	Young ice (gray ice, gray-white ice), 10–30 cm thick	–
3	Predominately new and/or young ice with some first year ice	–
4	Predominantly thin first year ice with some new and/or young ice	–
5	All thin first year ice (30–70 cm thick)	–
6	Predominantly medium first year ice (70–120 cm thick) and thick first year ice (>120 cm thick) with some thinner (younger) first year ice	–
7	All medium and thick first year ice	–
8	Predominantly medium and thick first year ice with some old ice (usually more than 2 m thick)	–
9	Predominantly old ice	–

Note. Ice concentration codes 1 and 8 were not included in analysis, as concentration was unclear.

commonly been used as a proxy for Palmer Station sea-ice conditions (e.g., Ducklow et al., 2013; Nardelli et al., 2023; Saba et al., 2014; Schofield et al., 2017, 2018).

To summarize sea-ice behavior and interannual variability, we used metrics defined by Stammerjohn, Martinson, Smith, and Iannuzzi (2008). Using a sea-ice year which begins on March 15th and ends March 14th the following year, we identified an annual day of ice-edge advance (DoA), defined as the first day in a five-day sequence where sea-ice concentration was at least 15% and remained above this threshold for five consecutive days, and day of ice-edge retreat (DoR), defined as the last day in the last five-day sequence where sea-ice concentration was above the 15% threshold for all 5 days. The sea-ice season duration is the total number of days elapsed between the DoA and DoR, and sea-ice persistence is defined as the percentage of days between DoA and DoR where sea-ice concentration is above the 15% threshold. These annual sea-ice metrics were computed for both in situ and satellite measurements.

To quantify late-winter in situ sea-ice variability, we defined an additional sea-ice metric: daily sea-ice variability in the window preceding DoR (referred to hereafter as sea-ice retreat variability). This metric identifies the number of days within the 60 days preceding the DoR where the concentration difference from one day to the next exceeded 35% (the largest possible difference between consecutive concentration bins, see Table 1). We limited the timing over which this metric is computed to the 60 days prior to the DoR, as we are primarily interested in the impacts of sea-ice variability and behavior toward the end of winter and into spring.

In conjunction with sea-ice concentration data, we used the Polar Pathfinder 25 km EASE-Grid (Tschudi et al., 2020; version 4) weekly-averaged sea-ice motion and velocity data from the closest grid cell to Palmer

Table 2
Endmember Values for Mass Balance Equations in Equation 1

	Salinity (S)	$\delta^{18}O$ (‰)
Meteoric water	0	−12
Sea-ice melt	7	+1.1
Circumpolar Deep Water	34.65	0

Station containing data (Figure 1a). Sea-ice speed and direction were computed from vectors derived from both satellite and buoy measurements. To obtain a weekly average, sea-ice data must be present for at least 4 of the 7 days each week. Sea-ice motion in each grid cell is dependent on the presence of ice in the immediate surrounding grid cells, and therefore sea-ice motion data is typically unavailable during times of patchy or short-lasting sea ice, as is often the case during the autumn and spring. These spatial and temporal requirements mean these data are a coarse approximation for sea ice behavior at the local scale, and instances when sea ice is patchy are not likely to be accurately represented in the data. Because this is currently the only approximation for direction and speed of sea ice motion, however, we use it with the understanding it is capturing the predominant winter sea ice motion in the region. Winter sea-ice motion averages were calculated using the weekly-averaged values throughout each sea-ice season to avoid timing inconsistencies present when defining the winter season by calendar months. Averaging of sea-ice motion was done using wind averaging conventions: u and v vector averages were computed individually for each sea-ice season, and the vector-average sea-ice speed and direction were computed using these averaged vectors.

2.2. Freshwater Sources

Oxygen isotope data, used to track sources of freshwater, were obtained and processed as in Meredith et al. (2021). Water samples were taken at a near-surface depth or 10-m depth at Stations B and E (Figures 1a and 2b) throughout the sampling season, beginning in sampling season 2011–2012. Samples were then analyzed for their oxygen isotopic composition using the CO_2 equilibration method (Epstein & Mayeda, 1953).

$\delta^{18}O$, or the standardized ratio of ^{18}O to ^{16}O, was then used in conjunction with salinity measurements to identify the relative contribution of meteoric freshwater input (glacial melt water or precipitation) and SIM input, as these two sources result in measurably different $\delta^{18}O$ signals. This calculation was done using a 3-endmember mass balance developed by Östlund and Hut (1984) for Arctic waters, and was adapted by Meredith et al. (2008) for the WAP, and assumes coastal water sources along the WAP originate from three distinct sources: meteoric water (Met), SIM, and modified Circumpolar Deep Water (CDW). The adapted balance equations are:

$$\begin{aligned} F_{\mathrm{Met}} + F_{\mathrm{SIM}} + F_{\mathrm{CDW}} &= 1 \\ S_{\mathrm{Met}}\ F_{\mathrm{Met}} + S_{\mathrm{SIM}}\ F_{\mathrm{SIM}} + S_{\mathrm{CDW}}\ F_{\mathrm{CDW}} &= S \\ \delta_{\mathrm{Met}} F_{\mathrm{Met}} + \delta_{\mathrm{SIM}} F_{\mathrm{SIM}} + \delta_{\mathrm{CDW}} F_{\mathrm{CDW}} &= \delta \end{aligned} \quad (1)$$

in which F_{Met}, F_{SIM}, and F_{CDW} are the fractions of meteoric water, SIM, and CDW of interest, S_{Met}, S_{SIM}, and S_{CDW} are the pure endmember salinities of each respective water source given in Table 2, and δ_{Met}, δ_{SIM}, and δ_{CDW} are the respective $\delta^{18}O$ values for each endmember. S and δ are the measured salinity and $\delta^{18}O$ of the sample. This mass balance results in frequent instances of negative SIM fractions, indicative either of local net sea-ice formation, which causes brine rejection and salinification, or of horizontal advection or vertical mixing of different water masses containing a similar net-sea-ice-formation signal.

2.3. Stratification

Conductivity, temperature, and depth (CTD) measurements were taken at coastal Stations B and E (Figures 1a and 2b) weekly or biweekly throughout the sampling season, which typically begins in October or November and continues through March of the following year. On average, CTD casts were taken to maximum depths of 63 m at Station B, and to 113 m at Station E. Sampling methods changed in 2008, resulting in a significantly shallower maximum sampling depth at both stations. At Station B, the average sampling depth was 68 ± 12 m for pre-2008 CTD casts, and 58 ± 8 m for post-2008 casts. At Station E, the average sampling depth was 148 ± 35 m pre-2008, and 80 ± 13 m post-2008. Individual profiles were binned to 1 m depth intervals, and further smoothed to account for instances when noise was not removed by binning. Smoothing was done using a Savitsky-Golay filter with a window size of 5.

Mixed layer depth was defined as the depth of the maximum Brunt-Väisälä frequency value (N^2) above the depth of the temperature minimum (T_{min}). This definition was determined to be the most ecologically-relevant MLD calculation along the WAP by Carvalho et al. (2017). Constraining the MLD to above the T_{min} depth ensures that the stratification features captured are products of current spring and summer processes and reduces the possibility of capturing a deep pycnocline. Stratification strength was determined by the maximum N^2 in a given CTD cast, where greater values indicate a greater relative density difference between a less-dense overlying water mass and the higher-density water below. A quality index based on methods derived from Lorbacher et al. (2006) and described in Carvalho et al. (2017) was used to identify the level of confidence of each MLD calculation, so that only instances of high and medium confidence were retained for further analysis. Further details on these methods can be found in Supporting Information S1.

2.4. Chlorophyll-*a*

Chlorophyll-*a* (chl-*a*) data were used as a proxy for phytoplankton biomass. Samples were taken approximately weekly, typically at six discrete depths at both Stations B and E throughout the sampling season. Station B was sampled to a maximum depth of 50 m, and Station E to a maximum depth of 65 m. Filtered samples were analyzed using a benchtop fluorometer or by using high-performance liquid chromatography (HPLC) as detailed in Saba et al. (2014). While greater temporal coverage of the fluorometrically analyzed chl-*a* exists over this time series, HPLC-analyzed chl-*a* is known to produce more accurate measurements. Because of this, we calibrated the fluorometrically-analyzed chl-*a* to the HPLC chl-*a* using a linear-regression model derived from instances where both measurements were present on the same sample ($p << 0.05$, $r^2 = 0.84$). This calibration equation allowed us to use the more widely available fluorometrically-derived chlorophyll-*a* with greater accuracy:

$$\text{Chlorophyll-}a_{\text{corr}} = \text{Chlorophyll-}a_{fl} * 0.5714 + 0.5175 \quad (2)$$

where chlorophyll-a_{corr} is the corrected chlorophyll value and chlorophyll-a_{fl} is the fluorometrically-derived measurement. Chl-*a* data are unavailable for sampling season 2007–2008.

Chl-*a* was integrated to 50 m at both stations. There are instances where the maximum sampling depth did not reach 50 m, particularly prior to standardized sampling protocols in 2008. Because omitting these sampling events would remove a significant amount of data, profiles which were sampled to at least a 15 m depth but not to 50 m were integrated to their deepest depth, consistent with methods from Saba et al. (2014). Instances where the deepest depth sampled was shallower than 15 m were not analyzed. Of the 802 analyzed chl-*a* profiles from Station B, there were 76 instances where the integration depth was at least 15 m but did not reach 50 m. Of the 754 profiles analyzed at Station E, there were 366 instances where the integration depth was at least 15 m but did not reach 50 m. The median depth for the analyzed profiles with integration depths shallower than 50 m was 35 m. As noted by Saba et al. (2014), this likely means integrated chl-*a*, especially in years preceding 2008, is slightly underestimated. In profiles sampled to at least 50 m over the entire record, the average chl-*a* maximum at Station B was 10.8 m, and at Station E was 11.9 m, suggesting that sampling to at least 15 m likely captured the chl-*a* maximum.

2.5. Averaging and Statistical Analyses

Based on analyses conducted in previous studies, we defined austral summer season to include December through February. We also defined austral spring from October to November. September was not included here because of the frequent lack of sampling data during September. Freshwater fractions derived from oxygen isotope samples, stratification, and chl-*a* data were averaged over both the spring and the summer. To limit the potential timing bias associated with averaging periods based on calendar months, we also computed averages over the entire sampling season and within the 60 days prior to and 30 days following the day of sea-ice retreat. We refer to this period as the sea-ice retreat-window. This allowed us to better understand physical and biological processes taking place at the time of sea-ice retreat. In addition to averages, we analyzed peaks in chl-*a* for the various time windows. We conducted simple linear regressions between two parameters and determined their significance by their p-value and r^2 value. Relationships were considered significant where $p \leq 0.05$. We report averages as mean ± one standard deviation.

Table 3
Means and Standard Deviations for In Situ and Satellite-Derived Sea-Ice Metrics

	In situ				Satellite			
Ice metric	Min	Max	Mean	Stdev (days)	Min	Max	Mean	Stdev (days)
Day of advance	Mar 15	Sept 5	June 30	47	May 21	Aug 9	July 6	23
Day of retreat	Aug 31	Mar 14	Nov 29	42	Sept 22	Feb 6	Dec 7	32
Sea-ice season duration (days)	19	311	152	67	72	228	155	42
Persistence (%)	56	100	77.0	12.9	69.4	100	92.3	7.2
Sea-ice retreat variability (days)	0	14	6	4	–	–	–	–

Note. Sea-ice retreat variability was not computed for the satellite sea-ice record. The in situ record spans from 1992 to 2020, and the satellite record spans from 1990 to 2021.

3. Results

3.1. Sea-Ice Metrics

In situ and satellite sea-ice metrics varied throughout the 30-year record (Table 3). In general, in situ sea-ice metrics exhibit higher interannual variability than those derived from satellite measurements, especially in the sea-ice season duration (Figure 3b) and persistence (Figure 3c). Satellite persistence is greater than in situ persistence by an average of 15% and exhibits lower interannual variability than the in situ record. The greatest sea-ice retreat variability was 14 days and occurred in 2004 and again in 2011. The 2005-2006 sea-ice year exhibited the longest sea-ice season duration (Figures 3a and 3b), which was accompanied by high persistence and only 2 days of high sea-ice retreat variability (Figures 3c and 3d).

Satellite observations from the Palmer Station 600.040 grid cell show a significant negative trend in the sea-ice season duration prior to 2009 ($p < 0.05$, $r^2 = 0.35$), consistent with regional studies (Schofield et al., 2018; Stammerjohn et al., 2008a, 2008b). However, this pre-2009 trend in the satellite record at this location is no longer significant when considering the entire time seriestime series. Unlike the satellite record, in situ sea-ice metrics do not exhibit significant trends when considering either the pre-2009 or the entire sea-ice record. In situ sea-ice shows a weak trend toward later ice-edge retreat over the entire record ($p < 0.1$, $r^2 = 0.12$; Figure 3a).

As indicated by the in situ sea-ice-type record, sea ice adjacent to Palmer Station is most commonly thin first-year sea-ice. The most reported sea-ice types are new ice, nilas, or young ice <30 cm (codes 0–2). Sea-ice type typically changes throughout the winter, beginning as a more immature form (new, gray, nilas, <30 cm) and maturing as the winter progresses to thin (30–70 cm) or medium-thick (70–200 cm) first-year ice (Figure S2 in Supporting Information S1).

3.2. Sea-Ice Motion

Satellite-derived weekly sea-ice velocity ranged from 0 to 14 cm s^{-1}. Weeks where sea-ice velocity exceeded 8 cm s^{-1} occurred exclusively when sea-ice was moving from the south/southeast (e.g., toward the north/northwest). Mean winter sea-ice velocity typically ranged from 1 to 4 cm s^{-1}, and mean winter sea-ice motion direction of origin typically ranged from 160° to 200°, indicating sea ice is typically moving from the southeast-southwest and toward the northwest-northeast throughout the winter (Figure 4). Winter averages consider both the frequency of direction as well as sea-ice velocity at the time of each measurement.

When winter sea-ice motion was predominantly northeastward, in situ sea-ice concentration at Palmer Station showed less daily variability around the time of sea-ice retreat (lower sea-ice retreat variability) compared to years when sea ice moved in a predominantly northwestward direction throughout the winter ($p = 0.005$, $r^2 = 0.25$). However, regionally (vs. locally), the satellite record shows that northeastward sea-ice motion throughout the winter was associated with later satellite-derived DoA, shorter satellite-derived sea-ice season duration, and lower satellite-derived sea-ice persistence, though interannual variability is high (Figure 5). No relationship was seen between winter sea-ice motion and timing of sea-ice retreat. This lack of relationship may be due to the unavailability of satellite-derived sea-ice motion data during the spring months caused by unresolved sea-ice motion or patchy sea-ice conditions.

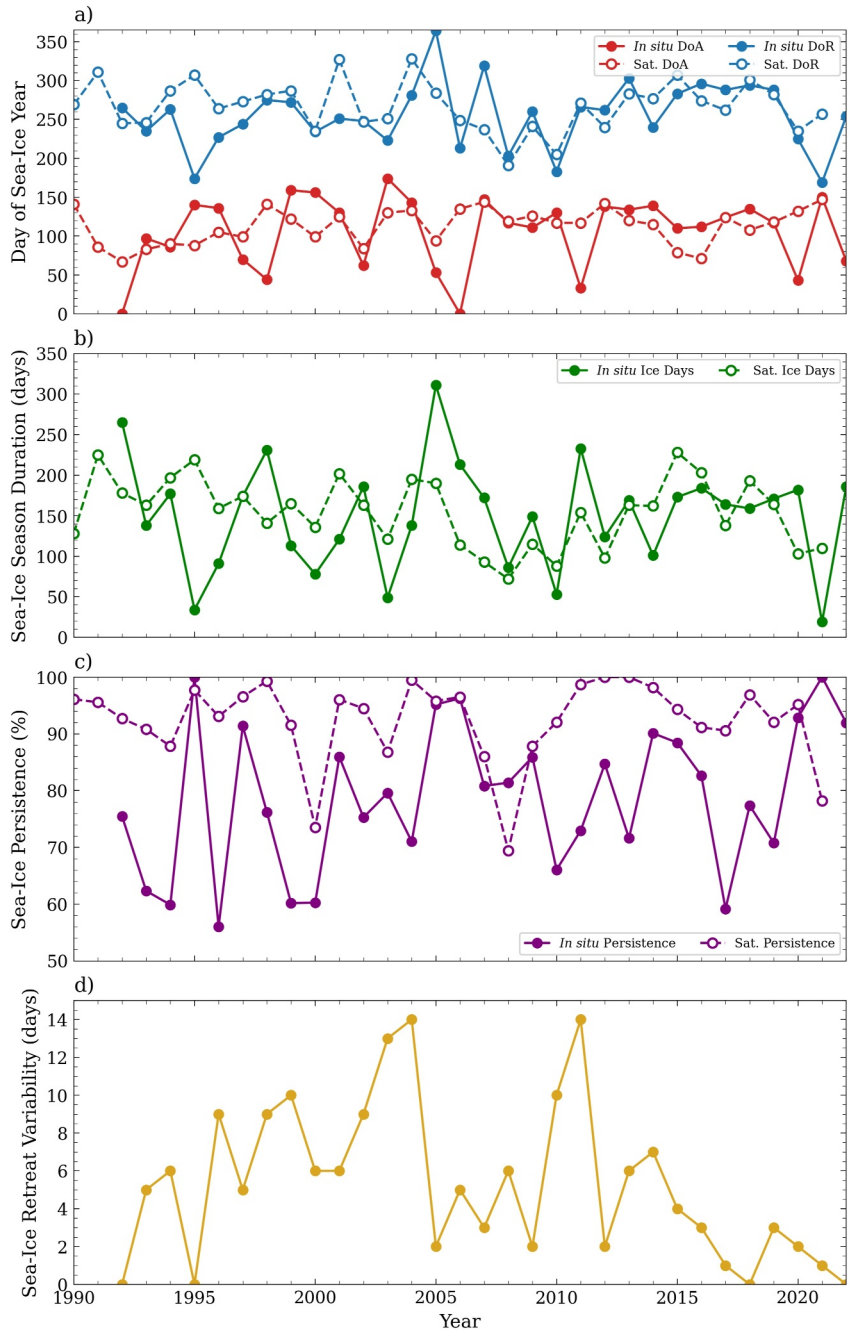

Figure 3. Sea-ice metrics for both in situ (solid) and satellite (dashed) sea-ice data. (a) Day of advance and retreat, (b) sea-ice season duration, and (c) sea-ice persistence. Also shown for the observed in situ record (d) sea-ice retreat variability (the number of days within the 60 days preceding the DoR where the concentration difference from one day to the next exceeded 35%).

3.3. Freshwater Sources

Isotopically-derived sea-ice and meteoric freshwater fractions exhibit strong seasonal cycles, as well as high spatial and interannual variability. Throughout the nine years of available oxygen isotope data, subsurface (10 m depth) SIM fractions at Station B averaged −0.26% ± 1.0%, with values ranging from −2.7% to +3.3% (Figure 6a). At Station E, the mean sea-ice fraction was −0.23 ± 1.0%, with values ranging from −5.2% to ±2.7%. Instances of SIM fractions greater than 3.3% occurred exclusively in Station B surface waters (approximately 0 m

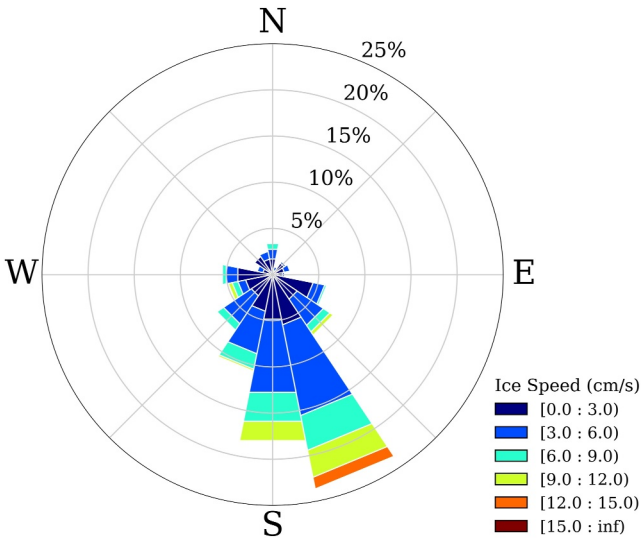

Figure 4. Sea-ice motion rose of all weekly data from the entire time series (1987–2021). Direction indicates sea ice direction of origin (ice moves toward the north/northwest throughout most of the record), with the length of each bar indicating the percentage of times ice is coming from that direction. Sea-ice velocity is shown by color.

depth). These surface samples at both stations are also where many of the most negative (lower than −2%) SIM fractions occurred. Negative SIM fractions indicate net sea-ice formation has taken place at that location (i.e., more sea ice grew in that location than subsequently melted in that location), as opposed to positive SIM fractions indicating net sea-ice melt.

Over the 9-year record, no significant trends were seen in the 10 m depth SIM fractions averaged over spring (October–November), summer (December–February), or in the sampling-season maximum (We note that only the 10 m depth data were used in these analyses since surface samples were not collected every year.) At both stations, sea-ice melt typically displays a seasonal peak at or just prior to the day of ice-edge retreat, followed by a decline throughout the spring and summer (Figure 6a). Years such as 2016–2017 are characterized by anomalously high sea-ice melt and a pronounced seasonal cycle (Figure 6a, Figure S3a in Supporting Information S1). In contrast, some years (e.g., 2014–2015) do not show a seasonal cycle, and SIM fractions remain low or negative throughout the sampling season (Figure 6a, Figure S3b in Supporting Information S1).

The 9-year mean subsurface meteoric fraction was 3.4 ± 0.75% and 3.3 ± 0.7% for Stations B and E, respectively. Throughout this period, meteoric water fractions ranged from 1.2% to 8.5%; however, instances of very high (>6%) meteoric fractions were limited to Station B surface water and are particularly prominent in sampling years 2015–2016 through 2017–2018. These instances of high meteoric factions are reflected in the salinity record as well, where anomalously low salinity values accompany these high meteoric fractions (Figure 6d).

At Station B, spring-averaged meteoric fractions, computed for 10-m sampling depth, exhibited an increase of 0.16% each year ($p < 0.05$, $r^2 = 0.75$). This trend was not seen at Station E. Neither summer-averaged nor sampling-season maxima meteoric fractions showed significant trends over time, perhaps indicating advection of spring meteoric water away from Station B. The meteoric freshwater signal also displays pronounced seasonality throughout the summer sampling season, typically exhibiting minima in early spring, and peaking toward the end of the austral summer (Figure 6b, Figure S3c in Supporting Information S1).

3.4. Physical Implications

One application of local-scale sea-ice analyses is to understand impacts on water-column stratification. Mixed layer depths and stratification strength adjacent to Palmer Station exhibited high variability on both interannual and shorter (days-weeks) time scales (Figure 7a). Stratification strength (Figure 7b) has increased since the beginning of the record, most prominently at Station E (Table 4). Over spring, summer, and the sea-ice retreat window (i.e., 60 days prior and 30 days after DoR), MLD shows a weak and statistically insignificant shoaling trend at both stations.

When utilizing in situ sea-ice metrics, we found that at Station B, later DoR was associated with higher stratification strength during spring, summer, and the sea-ice retreat window (Table 5, Figure 8a). Higher sea-ice retreat stratification strength was also associated with longer sea-ice season duration (Figure 8b). At Station E, higher stratification strength was characterized by later DoR and lower sea-ice retreat variability. We did not identify any significant relationships between in situ sea-ice metrics and MLD.

When using satellite-derived sea-ice metrics, later DoR was associated with higher stratification strength at Station E during the sea-ice retreat window ($p < 0.05$, $r^2 = 0.19$). However, this correlation was stronger and more significant using in situ sea ice metrics (Table 5). There were no other significant relationships found between stratification parameters and satellite-derived sea ice metrics.

No significant relationships were seen between annually averaged stratification parameters and sea-ice and meteoric freshwater fractions. Because there are only 9 years of available data, we also analyzed the relationship between sea-ice and meteoric fractions and stratification for each individual sampling event throughout the record. At the surface sampling depth (~0 m), both stations exhibited a strong positive relationship between

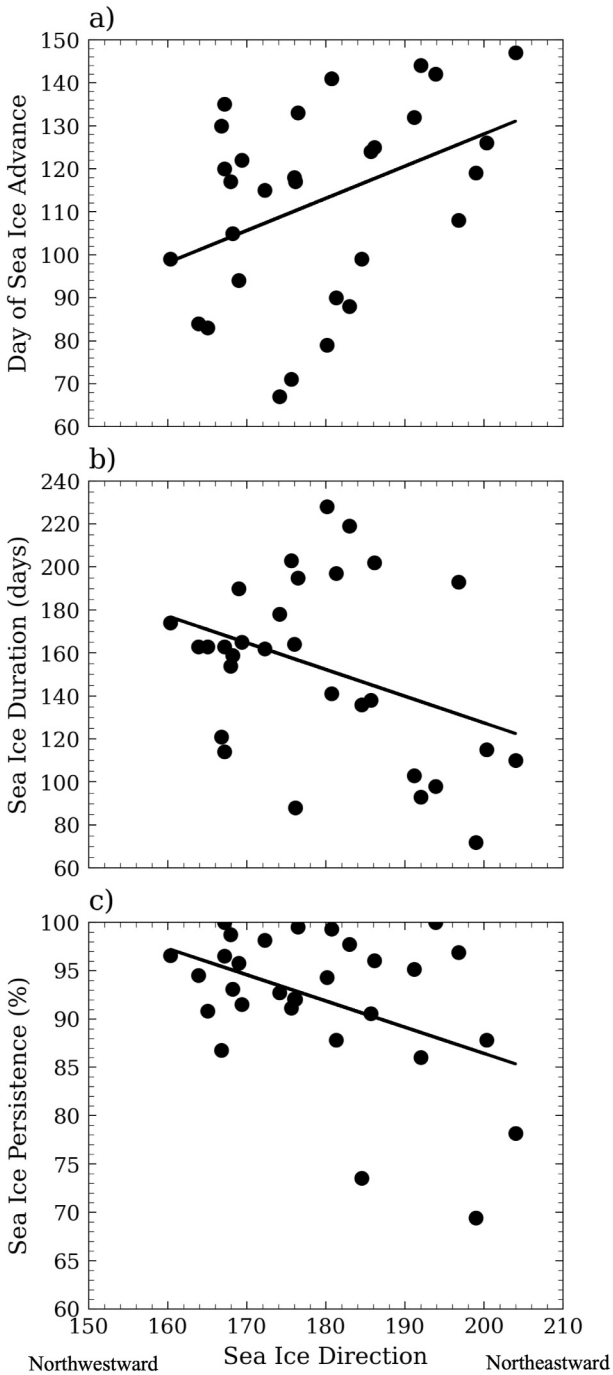

Figure 5. Impact of sea-ice direction of motion on satellite-derived day of sea-ice advance (a, $p < 0.05$, $r^2 = 0.16$), duration of sea-ice season (b, $p = 0.05$, $r^2 = 0.13$), and sea-ice persistence (c, $p < 0.05$, $r^2 = 0.19$). Sea-ice direction indicates the compass degree from where sea ice is coming (e.g., 210° indicates sea ice is coming from the southwest and moving toward the northeast).

meteoric freshwater and stratification strength (Station B: $p < 0.05$, $r^2 = 0.12$; Station E: $p << 0.05$, $r^2 = 0.49$). This relationship holds true at the 10 m sampling depth only at Station E ($p << 0.05$, $r^2 = 0.14$). We found no significant correlations between stratification and sea-ice fractions.

3.5. Biological Implications

Over the 30-year record, the average depth-integrated chl-*a* was 78 ± 62 mg m^{-2} at Station B, and 71 ± 46 mg m^{-2} at Station E. The 50-m integrated chl-*a* typically stayed below 200 mg m^{-2}, with values exceeding 200 mg m^{-2} occurring almost exclusively after 2008 (Figure 7c). Along with these higher chl-*a* peaks, the post-2008 record also exhibited higher interannual variability, particularly when considering chl-*a* maximums, which differed by 200–400 mg m^{-2} between years. Integrated chl-*a* typically exhibited one or two distinct peaks throughout the spring and summer sampling season, though the timing of these peaks greatly varied between years. The first of these peaks frequently occurred at or around the time of sea-ice retreat. Chl-*a* did not typically differ by more than 30 mg m^{-2} between stations.

Depth-integrated chl-*a* from 1992 to 2020 showed slight increases, particularly at Station B. When averaging around the sea-ice retreat window (60 days prior and 30 days after DoR), chl-*a* showed an increase of 2.5 mg m^{-2} $year^{-1}$ at Station B and 1.8 mg m^{-2} $year^{-1}$ at Station E (Table 6). The peak integrated chl-*a* during the sea-ice retreat window also increased significantly at both stations (Table 6). Additionally, Station B showed an increase in average summer chl-*a* and in sampling-season peaks. These trends were only weakly present at Station E. No trend was seen when analyzing spring-averaged chl-*a* at either station.

When conducting simple linear regression analyses to investigate the influence of sea-ice and water column dynamics on integrated chl-*a*, we found that higher peaks in integrated chl-*a* at Station E were associated with greater local sea-ice persistence (Table 7) and higher stratification strength during the sea-ice retreat window (Table 7, Figure 9). These same relationships were not present at Station B. We found no significant relationships between satellite-derived sea-ice metrics and chl-*a*.

4. Discussion

4.1. Sea Ice

Studies analyzing the interannual variability and longer-term decadal trends in sea ice at Palmer Station and along the Palmer Station LTER sampling grid previously used coarse-resolution satellite data (e.g., Saba et al., 2014; Stammerjohn et al., 2008; Stammerjohn et al., 2008). Here, we utilize previously unpublished in situ sea-ice data to improve our understanding of local-scale processes directly adjacent to Palmer Station. These in situ sea-ice metrics (DoA, DoR, sea-ice season duration, persistence) show higher interannual variability than metrics derived using satellite measurements. While the in situ observations may be subject to some level of observer bias and hence be less systematic, they better reflect the local-scale variability that is obscured by the 25-km resolution of the satellite measurements.

The in situ sea-ice record also demonstrates higher daily variability and more frequent oscillations between high and low sea-ice concentrations than the satellite record. The frequency of oscillations between high and low sea-ice concentrations also varied between years and is much better resolved in local observations than satellite. For

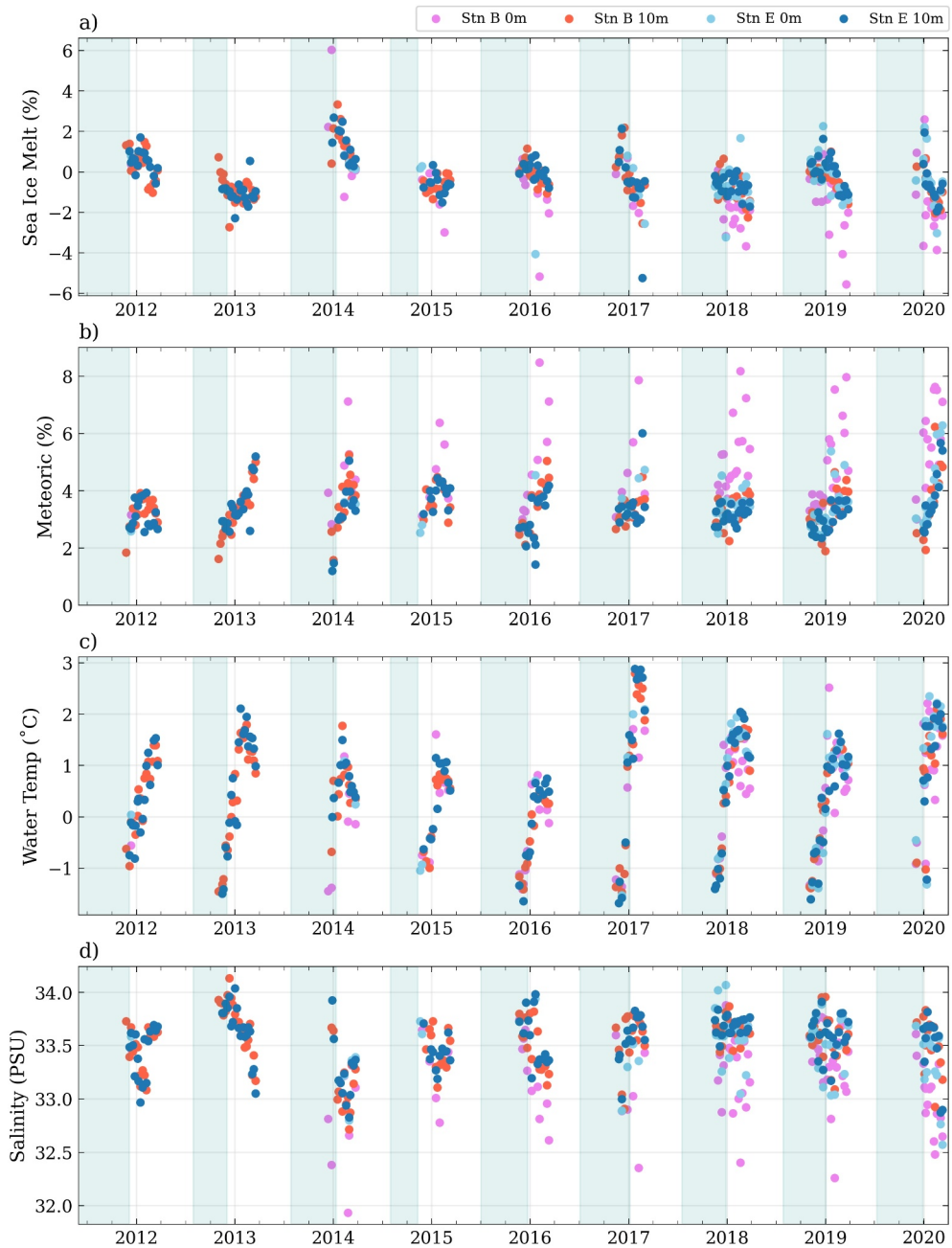

Figure 6. Time series of (a) sea-ice meltwater fraction, (b) meteoric freshwater fraction, (c) water temperature, and (d) salinity. The window of sea-ice presence between day of advance and retreat, as determined by the in situ sea-ice record, is shown with shaded blue portions.

example, sea-ice year 1999–2000 showed high daily variability, with sea-ice concentration decreasing fully to 0% for several days prior to returning to 95% for a similar period (Figure 10a). This high daily variability occurred prior to the official DoR. In contrast, sea-ice year 2016–2017 (Figure 10b) showed more consistent (i.e., less variable) daily sea ice coverage right up until the DoR. The sea-ice retreat variability metric is an attempt to quantify these differences on a time series-wide scale. We limited the timing over which this metric is computed to the 60 days prior to the DoR, as our focus was on the variability and impacts of sea-ice behavior on physical and biological conditions around the timing of sea-ice retreat. Sea-ice year 1999–2000 had 10 highly variable sea-ice days, whereas 2016-2017 had only 3. Future work in utilizing this metric may involve optimizing the threshold

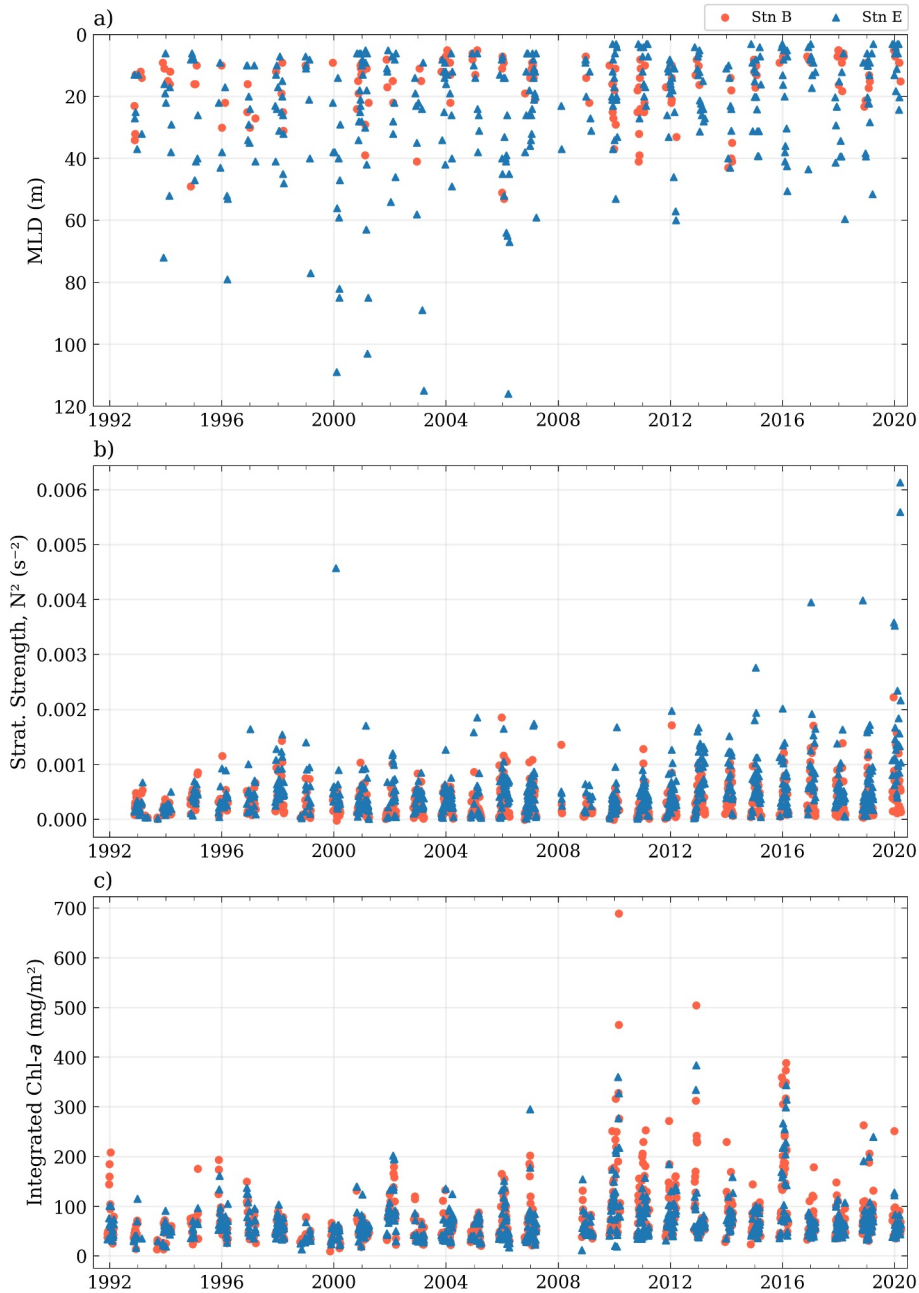

Figure 7. Time series of (a) Mixed layer depth, (b) stratification strength, and (c) integrated chl-*a* over the 30-year record at Stations B and E. Each point represents a single sampling event. Chl-*a* data was not available for 2007–2008 sampling year.

used, and redefining our methods to incorporate small data gaps, which are currently not tolerated in computing this metric.

The thin, patchy, and variable nature of sea ice around Palmer Station, shown by the sea-ice type and concentration record, demonstrates how higher-resolution observations are needed to capture highly variable local conditions, which, due to spatial and temporal averaging, are not always resolvable in the satellite record. In situ sea-ice observations offer an opportunity to complement the information provided by satellite observations and provide insights into the nuances of how local and nonlocal sea-ice dynamics interact to influence the coastal marine environment.

Table 4
Summary Statistics for Change in Stratification Strength and Mixed Layer Depth Over the 30-Year Record, for Each Annual Averaging Metric

		Stratification strength			MLD		
Averaging window	Station	p-value	r^2	Slope (s^{-2} $years^{-1}$)	p-value	r^2	Slope (m $year^{-1}$)
Spring	B	0.96	~0	1.3×10^{-7}	0.22	0.13	−0.45
	E	**0.006**	0.30	**1.2×10^{-5}**	0.08	0.16	−0.69
Summer	B	**0.037**	**0.16**	**7.1×10^{-6}**	0.27	0.05	−0.14
	E	**4.7×10^{-5}**	**0.46**	**2.1×10^{-5}**	0.21	0.06	−0.25
Sea-ice retreat window	B	0.31	0.05	6.9×10^{-6}	0.35	0.04	−0.31
	E	**0.026**	0.20	**2.2×10^{-5}**	0.19	0.08	−0.5

Note. Sea-ice retreat window is the period 60 days prior and 30 days after DoR. Bolded values are statistically significant.

4.2. Sea-Ice Motion and Meltwater

Sea-ice motion, derived from satellite and buoy data, provides an additional way to understand sea-ice behavior. Offshore of Palmer Station, sea ice moves in a predominantly northward direction throughout the winter. We found that northeastward sea-ice motion, more so than northwestward sea-ice motion, was associated with lower in situ sea-ice retreat variability (more consistent sea-ice pack preceding retreat). More northeastward sea-ice motion exhibited the opposite effect on satellite sea-ice metrics, however, showing that northeastward motion was associated with later advance, shorter sea-ice duration, and lower persistence. These same relationships were not seen when looking at in situ sea-ice metrics, likely due to the dissimilarity in scale between the satellite sea-ice motion and local in situ sea-ice metrics. The differing response of in situ sea-ice metrics to sea-ice motion (lower sea-ice variability in years of northeastward sea-ice motion) highlights how, while regional sea-ice observations may not always capture local nuances, regional-scale dynamics exert influence on local-scale conditions. Satellite-derived sea-ice metrics and motion, used in conjunction with local-scale observations, provide insight into the impact of regional sea-ice behavior on local-scale sea-ice behavior.

Isotopically-derived SIM fractions fluctuate throughout each sampling season, and frequently differ between Stations B and E. The declines in SIM fractions seen in the middle of the summers, when sea ice is consistently absent, indicate that localized episodic vertical mixing events or horizontal advection of isotopically different water masses play an important role in determining the sea-ice melt signal and may obscure direct relationships between sea-ice metrics and meltwater.

The dominance of low and negative sea-ice melt fractions throughout the record indicates that the waters around Palmer Station are commonly sites of net sea-ice formation. Years where SIM fraction does not increase in the spring in conjunction with sea-ice retreat imply that the sea ice which formed at this location throughout the winter (causing a negative meltwater signal) was likely advected away before melting, indicating a dynamic form

Table 5
Linear Regression Statistics for Three Different In Situ Sea-Ice Metrics and Stratification Strength Over Different Averaging Periods

		DoR		Ice season duration		Sea-ice retreat variability	
Averaging window	Station	p-value	r^2	p-value	r^2	p-value	r^2
Spring	B	**0.03**	**0.2**	0.09	0.12	*0.52*	*0.02*
	E	0.69	0.15	0.44	0.03	***0.05***	***0.17***
Summer	B	0.01	**0.2**	0.06	0.13	*0.07*	*0.12*
	E	0.15	0.07	0.58	0.01	*0.47*	*0.02*
Sea-ice retreat window	B	**6.7×10^{-5}**	**0.56**	**0.04**	**0.2**	*0.39*	*0.04*
	E	**1.7×10^{-3}**	**0.36**	0.22	0.07	*0.3*	*0.05*

Note. Bolded values are statistically significant. Italicized values indicate the relationship had a negative slope. Bolded values are statistically significant, italicized values indicate the relationship had a negative slope.

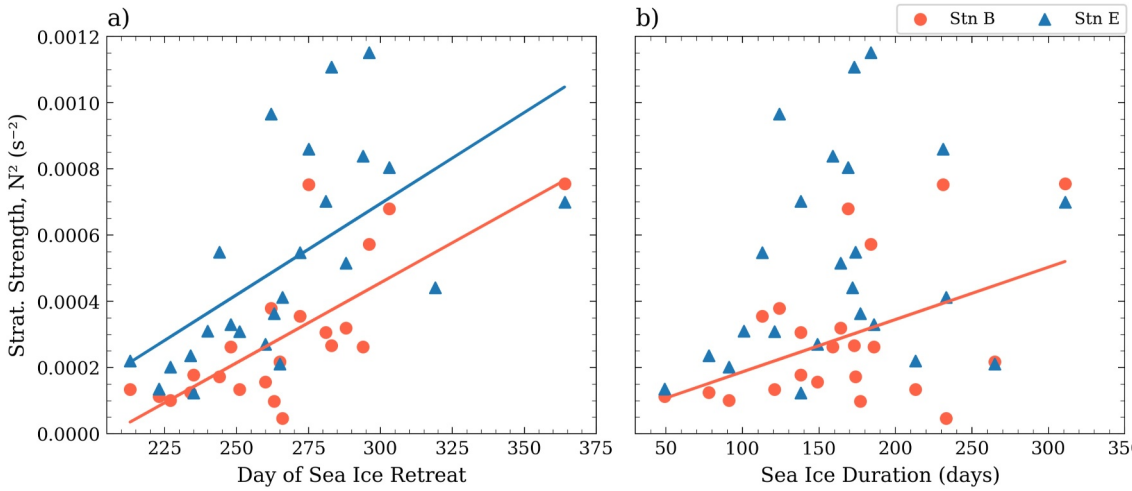

Figure 8. Average stratification strength during the sea-ice retreat window as predicted by in situ (a) sea-ice DoR and (b) sea-ice duration.

of sea-ice retreat. These years exhibiting different meltwater behavior highlight how sea ice presence around Palmer Station does not necessarily lead to large meltwater influxes upon spring retreat.

Case years utilizing these isotope data are explored by Meredith et al. (2013, 2017). These studies attribute years of predominantly negative SIM fractions to the Palmer Station region acting as an "ice factory," or site of net sea-ice formation. From the high sea-ice melt seen along the WAP south of Palmer, they infer that sea ice formed around Palmer Station moves predominantly southward along the peninsula, where it then melts (Meredith et al., 2013). Meredith et al. (2021) explores 2 years of particularly high SIM fractions. In 2013–2014, they attributed high SIM to offshore (northwestward) sea-ice motion which extends the sea-ice edge, creates firm pack, and leads to large amounts of sea ice melting in place. In 2016–2017, higher sea-ice fractions were attributed to onshore (northeastward) sea-ice compaction. In addition to utilizing oxygen isotope data from Stations B and E throughout the sampling season, Meredith et al. (2021) analyzed data from the Palmer Station sea-water intake, taken throughout the winter for several years (2013–2017). From these data, they identify the importance of year-round sampling to capture rapidly changing freshwater dynamics. While we were unable to include year-round sampling in our time series-long analysis due to the limited number of years available, continued collection and analysis of year-round data would provide immense value in better understanding local impacts of sea ice formation and retreat.

We expand on this 2-year study by analyzing sea-ice presence, meltwater fractions, and winter motion collectively across the 9-year oxygen isotope record. We find that, although the sea ice moves predominantly northwestward throughout the entire time seriestime series, differences in sea-ice motion arise between years that

Table 6
Summary Statistics for Change in Integrated Chl-a Over the 30-Year Record, for Each Annual Averaging and Maxima Metric

Time window	Station	p-value	r^2	Slope (mg m^{-2} $year^{-1}$)
Summer (Dec-Feb) average	B	**0.03**	**0.17**	**1.93**
	E	0.16	0.07	0.88
Sea-ice retreat window average	B	0.01	**0.27**	**2.12**
	E	**0.04**	**0.2**	**1.38**
Sampling season peak	B	0.01	**0.22**	**7.85**
	E	0.07	0.12	3.5
Sea-ice retreat window peak	B	**0.002**	**0.37**	**8.35**
	E	**0.02**	**0.23**	**4.68**

Note. Sea-ice retreat window is the period 60 days prior and 30 days after DoR. Bolded values indicated a statistically significant relationship. All relationships were positive.

Table 7
Summary Statistics for Linear Regressions on Station E Integrated Chl-a Based on In Situ Sea-Ice Persistence and Stratification Strength

	Persistence		Stratification strength	
Time window	p-value	r^2	p-value	r^2
Sea-ice retreat window average	*0.76*	*0.005*	0.05	0.08
Sampling season peak	0.03	0.17	0.36	0.04
Sea-ice retreat window peak	0.73	0.006	0.02	0.22

Note. Sea-ice retreat window is the period 60 days prior and 30 days after DoR. Italics indicate a negative relationship. No significant relationship was seen at Station B for these parameters.

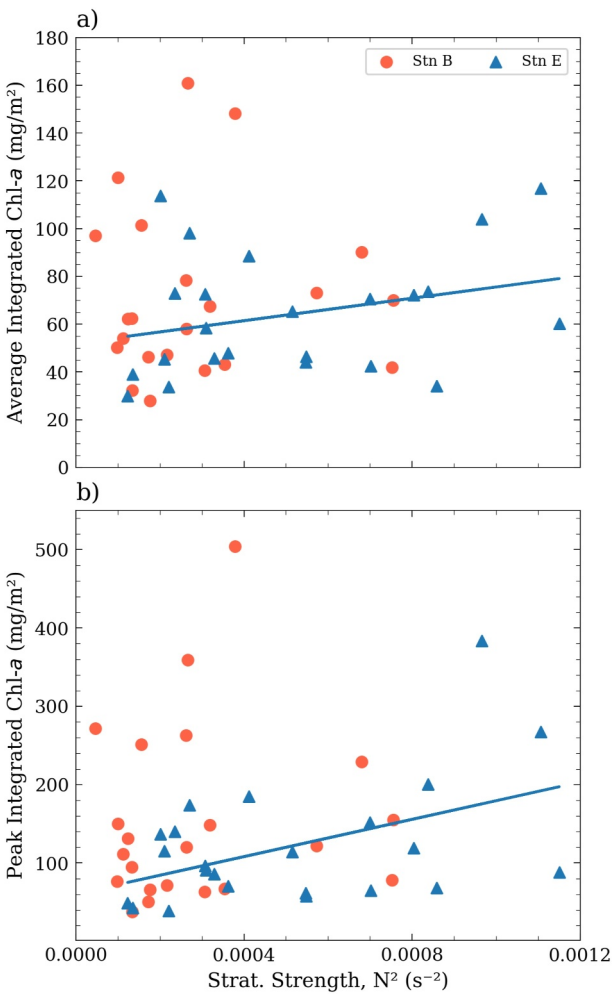

Figure 9. Impact of stratification strength on both the average (a) and peak (b) integrated chl-*a* during the sea-ice retreat window.

display a clear increase in SIM fractions in the spring, and those that do not (Figure 11). Years exhibiting a pronounced, positive meltwater signal around the time of ice-edge retreat (2011–2012, 2013–2014, 2015–2016, 2016–2017, 2019–2020), are characterized by predominantly fast, northwestward sea-ice movement, with less than 10% of all sea-ice motion moving in a southward direction (Figure 11, bottom row). In contrast, years where SIM remains primarily negative or display no clear spring peak (2012–2013, 2014–2015, 2017–2018) show highly variable direction of sea-ice motion, accompanied by generally lower sea-ice velocity (Figure 11, top row). Examples of contrasting years are shown in detail Figures S3a, and S3b in Supporting Information S1.

This observation expands the hypothesis presented by Meredith et al. (2021) to all years showing positive SIM peaks. A dominance of north or northwestward sea-ice motion may be causing offshore extension of the sea-ice edge, increasing the volume of sea ice, which then melts in place each year and causes distinct meltwater peaks. Years which are preceded by winters of slower and more directionally-variable sea-ice motion typically lack these meltwater influx signals, potentially indicating a lack of ice-edge extension and an overall patchier sea-ice pack. Additionally, years lacking spring meltwater peaks may be a result of southward sea-ice transport away from Palmer Station, given the relatively higher instances of southward sea-ice motion, and following inferences made in Meredith et al. (2013).

The one exception to this pattern is the sample year 2018–2019 (Figure 11, Figure S3c in Supporting Information S1), which shows a somewhat broad sea-ice melt peak during the spring, indicating a considerable amount of sea ice melted in situ around Palmer Station. However, the variability of sea-ice direction of motion is more similar to those years which do not display a pronounced SIM signal. In looking at weekly sea-ice motion data, however, we see that the bulk of winter is characterized by sustained northward sea-ice motion, especially at times of high velocities, likely extending the ice-edge. The fast northeastward sea-ice movement seen at the very end of winter may have caused compaction of sea ice along the shore, effectively shrinking total sea-ice area, but potentially increasing the volume of sea-ice via dynamic rafting, that subsequently melted in situ, creating the distinctly broad spring peak in SIM.

Despite the highly local nature of the SIM fractions and in situ observations, and the relatively nonlocal nature of sea-ice motion data, we see a clear link between the preceding winter's sea-ice behavior and resulting SIM pulses in the spring. These connections display how the local Palmer Station environment is influenced not only by local sea-ice behavior (i.e., high variability captured in the in situ record) but also by regional sea-ice dynamics, and highlight the importance of multi-scale analyses of sea-ice behavior.

Identifiable influences of sea-ice motion on local-scale SIM are limited by sea-ice motion data availability, which requires a minimum amount of continuous sea-ice pack, and therefore does not necessarily capture sea-ice motion during times of patchy sea ice (i.e., during spring ice-edge retreat) even though all available data was included in our analysis rather than limiting to a calendar month definition of winter. As identified in Meredith et al. (2021), sea-ice motion remains fairly homogeneous (i.e., same direction) over large spatial scales, particularly during strong wind events. A direction of future research could be to expand the spatial range over which sea-ice motion is analyzed to increase the likelihood of acquiring detectable sea-ice motion data later into the spring, which, by the findings of Meredith et al. (2021), would allow us to make inferences about the near-Palmer Station

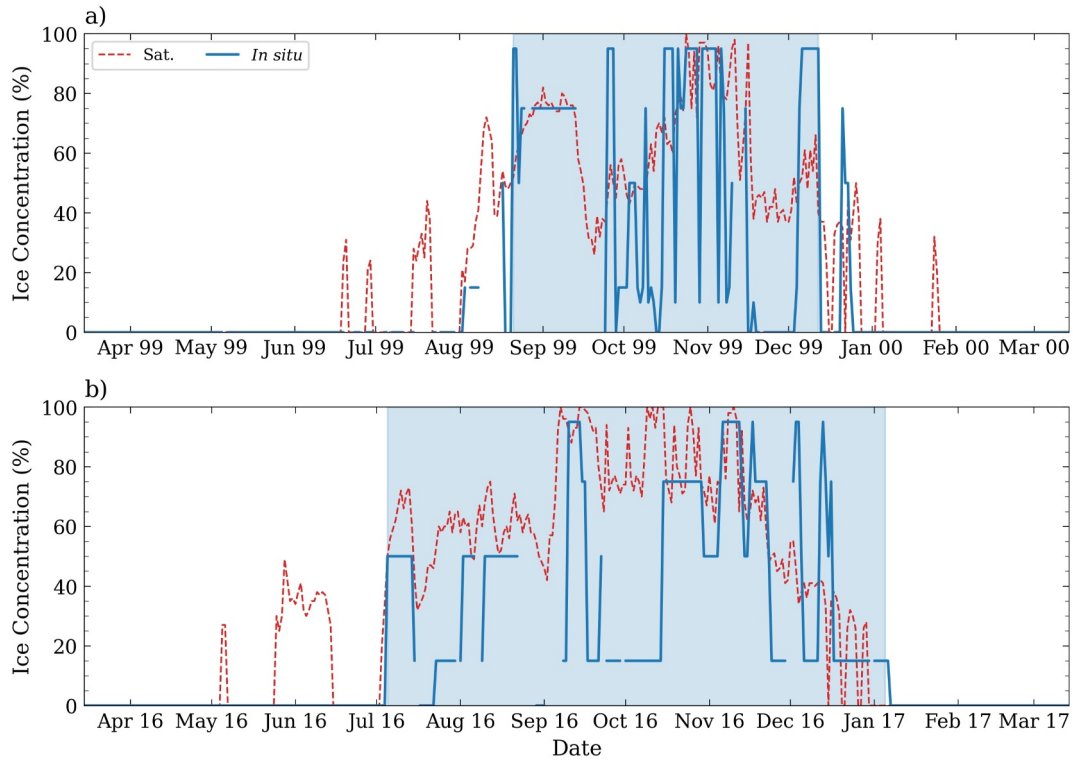

Figure 10. Ice concentration recorded by in situ observations (Obs.) and by satellites (Sat.) for two sea-ice years: (a) 1999–2000 and (b) 2016–2017. The window of sea-ice presence between day of advance and retreat, as determined by the in situ sea-ice record, is shown with shaded blue portions.

sea-ice motion, and provide additional insights into the interpretation of spring and summer SIM variability adjacent to Palmer Station.

4.3. Physical Implications

Previous studies have found that coastal physical and biological processes are closely linked to sea-ice dynamics, and help explain the high rates of primary production along the WAP, and this region's role in sustaining higher trophic level processes (Ducklow et al., 2007; Saba et al., 2014). Many of these studies have linked higher concentrations of summer photosynthetic biomass to years with higher sea-ice the preceding winter, hypothesizing that extended sea-ice presence both insulates the water column from wind-driven mixing and releases fresh, buoyant meltwater into the surface ocean upon melting, which can lead to shallower mixed layer depths and greater light availability (Ducklow et al., 2013; Vernet et al., 2008) or changes in the stratification and potential for mixing below the mixed layer (Venables et al., 2013).

A common feature of these previous studies, with the exception of Venables et al. (2013), has been the usage of the satellite records in determining sea-ice behavior. However, as we see when comparing the in situ and satellite sea-ice records, variability seen at the local scale is not fully captured by the coarse-resolution satellite data, and it is challenging to determine both if and how sea ice is impacting the coastal water column. By pairing satellite sea-ice observations with regional sea-ice motion, in situ concentration and type, and SIM fractions, we attempt to build a more comprehensive understanding of the mechanistic links between sea ice and stratification.

When looking at the 30-year MLD and stratification strength record, we detected a clear increase in stratification strength at Station E when averaged over the spring, summer, and sea-ice retreat window. Summer-average stratification strength at Station B also showed an increasing trend. Stratification strength was most strongly associated with in situ sea-ice DoR, sea-ice duration, and variability around the time of sea-ice retreat. These relationships follow previous hypotheses which indicate greater sea-ice coverage leads to a more stratified water column, although these studies focused on MLD (Schofield et al., 2018; Venables et al., 2013), while here we

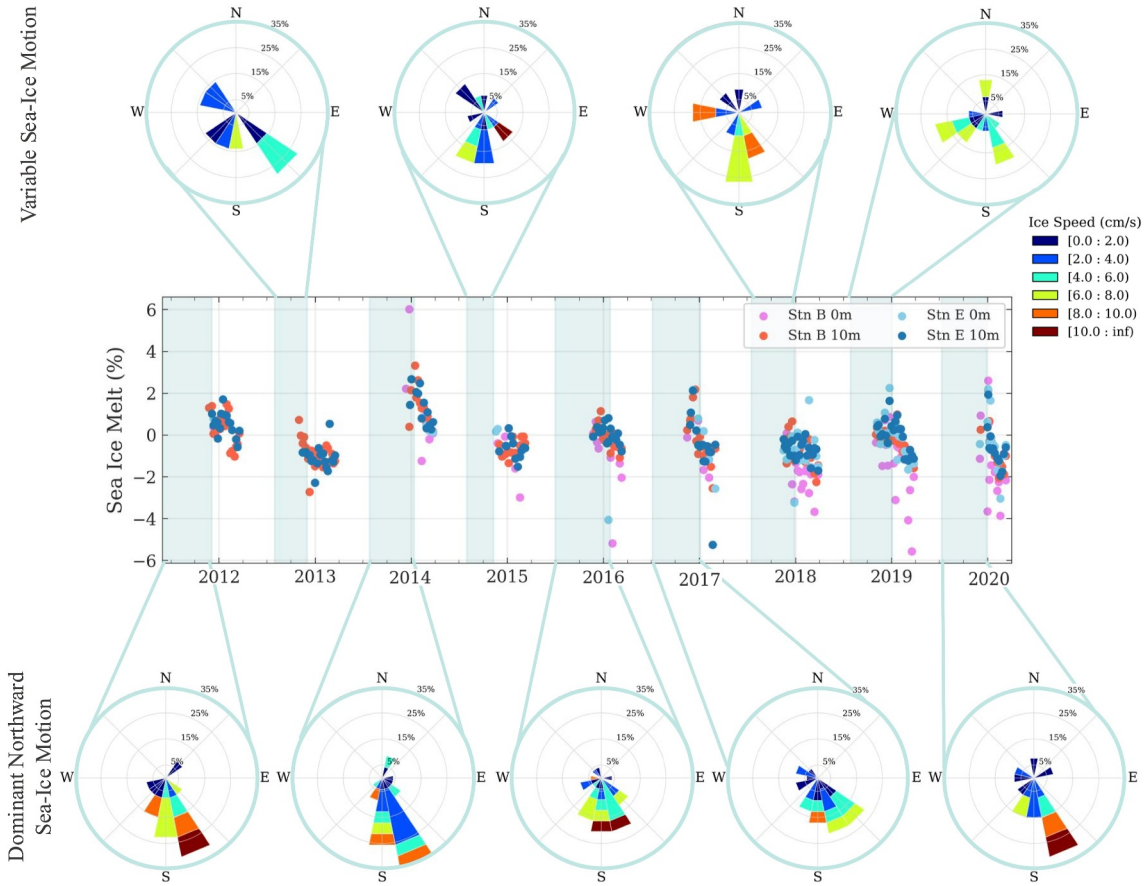

Figure 11. Sea-ice meltwater fractions and the previous year's sea-ice behavior at Stations B and E. Shaded regions indicate the sea-ice season window as determined by the in situ record. Sea-ice motion roses for each sea-ice season are shown on the top and bottom. For each ice motion rose, the direction indicates sea-ice direction of origin, with the length of each bar indicating the percentage of times sea ice is coming from that direction. Percentages are indicated by numbered concentric circles. Ice velocity is shown by color. Years with strong, dominantly northward sea-ice motion are shown in the bottom row, and years with more varied sea-ice motion are shown on the top row.

identify stratification strength as a parameter with stronger correlations to local-scale nearshore sea-ice behavior. Importantly, we do not see these same relationships reflected in the satellite sea-ice record, highlighting the importance of looking at multiple scales of sea-ice behavior to understand the impact on the physical water column. The importance of sea-ice variability during the time of sea-ice retreat has also not been previously quantified and highlights how variability, in addition to timing, can influence stratification, likely by irregular and more frequent exposure to wind-mixing.

As mentioned, sea-ice presence can influence water column stratification by physically protecting the surface ocean from wind-driven mixing, or by releasing dense, high-salinity brine during ice formation, or by releasing fresh, buoyant water during ice melting. The oxygen isotope record on the other hand provides an opportunity to isolate the subsequent influence of SIM on water column structure once the sea ice has melted. At the sampling event scale, we saw that greater stratification strength was associated with higher meteoric meltwater fractions, with increasing trends observed in both spring meteoric water and summer stratification strength at Station B (the station closest to land). These results may indicate that the influence of meteoric meltwater inputs into the coastal WAP system may be playing an increasing role in water column stratification, as glacial runoff continues to increase (Wallis et al., 2023). However, the lifespan of meteoric water at Station B appears to be short and over the 9-year oxygen isotope record, we found no direct correlations between annually-averaged sea-ice or meteoric freshwater fractions and annually-averaged stratification parameters.

Given that more extensive sea-ice presence correlated with increased stratification strength, we might also expect that SIM fraction might be correlated with stratification strength, but there is no such correlation. Either there is

not a long enough record to see a statistically significant relationship given high interannual variability and multiple controls or the connections between in situ sea-ice metrics and stratification strength are a result of the insulation effect from wind-driven mixing, rather than the stratifying effect of SIM. This lack of correlation is however consistent with the observation that the area adjacent to Palmer Station has been characterized as an area of net sea-ice production, where sea-ice growth during winter is not balanced by sea-ice melt during spring due to wind-driven processes driving sea-ice out of this area during spring retreat (Meredith et al., 2021). In short, identifying the mechanism through which sea ice may impact coastal stratification (i.e., through meltwater influx or wind insulation) would not be possible without the presence of oxygen isotope-derived meltwater fractions. Although the oxygen isotope record does not contain as many years of data, we see a clear influence of meteoric meltwater on stratification but do not identify a similar influence of SIM.

4.4. Biological Implications

Between 1992 and 2020, we observed an increase in the average and peak depth-integrated chl-*a* at both stations during the period around ice-edge retreat, as well as an increase in summer-averaged (December–February) and sampling-season peak chl-*a* at Station B. This increasing trend is consistent with several prior studies, though those studies differed in their suggested driving mechanism. Montes-Hugo et al. (2009) documented increasing chl-*a* from 1978 to 2006 in the southern WAP (south of Palmer Station), and attributed higher chl-*a* to decreases in sea ice that favored increased light availability in spring (i.e., the long sea-ice seasons in the southern region had been light-limiting for phytoplankton). Schofield et al. (2018) attributed increased carbon fixation and photosynthetic efficiency to shallower MLD in the northern region of the WAP, although did not identify significant changes in photosynthetic biomass, or a direct correlation to sea-ice changes. Saba et al. (2014) and Schofield et al. (2017) examined satellite-observed sea ice and primary production using nearshore chl-*a* data from Palmer Stations B and E, though over slightly different times cales. Both studies concluded that increases in satellite-observed sea ice led to increased summer chl-*a* via shallower mixed layer depths, although Schofield et al. (2017) noted that, even during periods of sea-ice decreases, chl-*a* showed high variability and slight increases.

In this study, sea-ice metrics and stratification parameters do not fully explain variability or increasing trends in photosynthetic biomass. We found that, at Station E, higher in situ sea-ice persistence and strength of stratification both led to larger peaks in integrated chl-*a*. Notably, no ice influence on integrated chl-*a* was seen when using satellite-derived sea-ice metrics, indicating the importance of including local-scale sea-ice observations when considering how the ice environment impacts coastal biology.

The identified impact of meteoric freshwater on stratification strength highlights a potential driver behind the increase in chl-*a*. It is known that glacial melt along the WAP has increased over the past 30 years (Cook et al., 2016) and is likely to continue to increase (Wallis et al., 2023). Prior studies have hypothesized increased glacial melt may lead to greater primary production, as glacial melt provides a source for micronutrients such as iron (Eveleth et al., 2017; Schofield et al., 2018; Smith et al., 2011). Our results showing both an increase in spring meteoric freshwater, as well as an influence of this freshwater on stratification strength, indicate that meteoric water may contribute to increased phytoplankton biomass by influencing stratification strength, and potentially by supplying limiting nutrients. Increasing meteoric influx and stratification strength may also impact the species distribution of phytoplankton in the coastal waters. For example, Mendes et al. (2023) found that elevated light stress caused by shallow, well-stratified mixed layers led to greater amounts of cryptophytes and fewer diatoms. Future changes in freshwater inputs and stratification in coastal waters may lead to more prolonged changes in phytoplankton dynamics and ultimately significant changes in biological carbon drawdown and food availability for higher trophic levels (Brown et al., 2019; Mendes et al., 2023).

We also found that longer sea-ice seasons led to lower spring chl-*a*, consistent with the earlier years analyzed by Schofield et al. (2017), though this study utilized time-integrated chl-*a* and satellite-derived sea-ice metrics. This contradicts the idea that a higher-ice year leads to great chl-*a* biomass, and is potentially a product of sample-timing bias, where longer sea-ice seasons push back the start of sampling, and therefore early (and potentially substantial) blooms in October or November may not be captured.

Sea-ice retreat and peaks in meltwater and chl-*a* vary substantially from year to year in relation to the calendar, causing limitations when attempting to define averages based on calendar months (i.e., defining "spring averages" to be within October and November). In attempting to better constrain the drivers of variability in early spring chl-

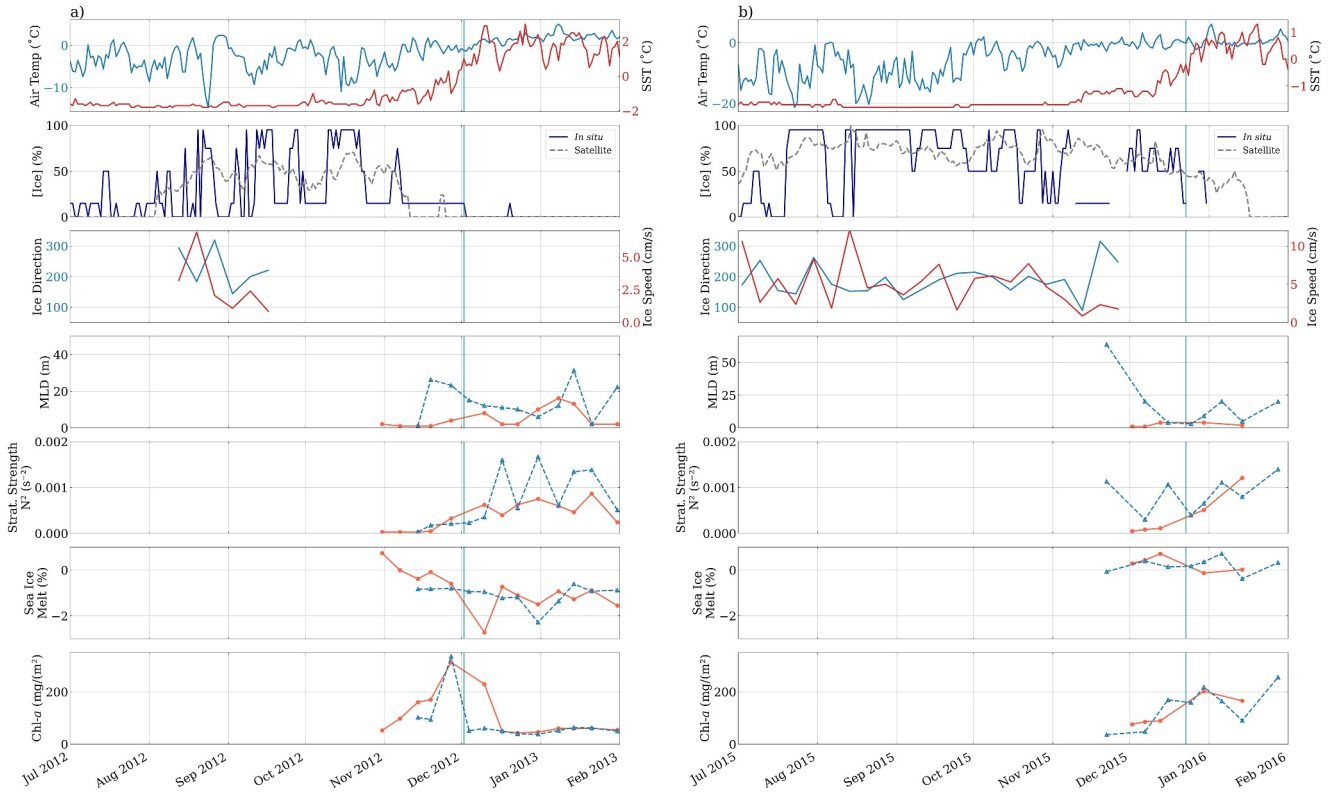

Figure 12. Time series of temperature, ice conditions, ice direction of origin, stratification, and chl-*a* in 2012–2013 (a) and 2015–2016 (b). The vertical blue line shows the DoR as defined by in situ ice observations.

a peaks, understanding that blooms do not adhere to calendar-based definitions of seasons, we defined an additional averaging window for chl-*a* based on the timing of sea-ice retreat. It is clear from looking at each individual ice year that the timing of chl-a peaks is linked to sea ice dynamics with blooms typically occurring on or just prior to the defined day of sea-ice retreat. By analyzing chl-*a* within this sea-ice retreat window, we were able to see more directly relevant influences (sea-ice persistence and stratification strength) on integrated chl-*a*. This approach to understanding coastal processes based on the timing of environmental events such as sea-ice retreat, rather than calendar months, may provide valuable future insights into mechanistic influences on phytoplankton behavior.

While in situ sea-ice persistence and stratification strength show some influence on the magnitude of these blooms, they do not explain a large portion of the variability seen, highlighting the complexity of this coastal system. The lack of a dominant driver in chl-*a* dynamics throughout the entire season indicates that the degree of influence of each environmental condition (i.e., local and regional sea ice, freshwater influxes, and stratification) may vary between years. To better understand the variation in drivers of chl-*a* between years, we identified two case study years, 2012–2013 and 2015–2016. Both years exhibit a high (>350 mg m^2) peak in chl-*a* just prior to the day of sea-ice retreat; however, differences in ice and environmental conditions between these two years point to the possibility of different bloom mechanisms. In particular, one of these exhibited high SIM influx, while the other exhibited no significant SIM influx.

Sampling year 2012–2013 had relatively high sea-ice persistence and low variability around the time of sea-ice retreat, with ice remaining present up until the DoR (Figure 12a). This year exhibited only two highly variable sea-ice days in the 60 days prior to DoR. Sea ice retreated both locally and regionally within 22 days of each other. 2012–2013 was also characterized by primarily negative SIM fractions. This sustained presence of ice, coupled with the almost exclusively negative SIM fraction, indicates sea ice may have formed in this location but did not likely melt in this same place. Mixed layer depth remains consistently shallow (<20 m) at both stations during this period, and stratification strength increases throughout November and December. The fact that the increase in stratification strength takes place several weeks following the initial peak in chl-*a*, and that MLD remains

constant throughout this window, indicates that the chl-*a* peak was not a product of some strengthening or shoaling of the mixed layer. Instead, we hypothesize this peak occurred as a direct result of the sudden increase in light following the retreat of a fairly extensive sea-ice cover.

Like 2012–2013, sampling year 2015–2016 had a long sea-ice season (173 days), with a slightly greater number of highly variable ice days in the 60 days prior to sea-ice retreat (4 days total). The DoR as determined by in situ observations is 24 days prior to that determined by satellite data, and better corresponds to the timing of the bloom. In contrast to sampling year 2012–2013, 2015-2016 showed relatively high SIM fraction, especially at Station B (Figure 12b). Sea-ice meltwater fractions at Station B were positive throughout the beginning of the sampling season, likely caused primarily by an extension of the sea ice edge followed by thermodynamic melting in place, consistent with the dominantly north-northwestward ice motion during this season. Accompanying this increase in sea ice melt at Station B is a slight increase in stratification strength, coinciding with a peak in chl-*a*. The relatively close timing of this influx of meltwater and peak in chl-*a* highlight a different mechanism for bloom initiation than the one seen in 2012–2013. The peak in chl-*a* concentration at Station B appears to be due to an influx of buoyant SIM, rather than just a light response. Sea ice in the broader region around Palmer Station, even if not present locally could supply meltwater that advects closer to our measurement site throughout January. The meltwater may help phytoplankton remain in the photic zone, could seed the bloom with ice algae and/or deposit ice-suspended nutrients.

These case years lead us to hypothesize that phytoplankton blooms along the WAP shelf can be triggered by sea ice both directly, by modulating the timing of light availability as sea ice retreats, and/or indirectly, by the insulative effect from wind mixing and/or by SIM inputs that modulate MLD and upper ocean stratification. These mechanisms are likely to vary from year to year, and the presence or absence of a large influx of SIM in spring is not the sole driver in determining the fate of the spring bloom. Saba et al. (2014) presented similar hypotheses, but the addition of meltwater data allows us to see the degree of influence of each physical characteristic from year to year and helps to further explain the lack of correlation between sea-ice melt and chl-*a* dynamics over the entire record.

5. Conclusions

Previous studies of the impacts of sea-ice variability on marine productivity along the WAP shelf have focused primarily on time series analysis of regional sea-ice metrics. Here, we augment the commonly utilized satellite sea-ice concentration record with satellite-derived sea-ice motion, as well as with local observations acquired near Palmer Station, including in situ sea-ice concentration and meteoric and SIM fractions isotopically-derived from locally acquired seawater samples. Local-scale sea-ice dynamics provide insight into the highly variable environment experienced by the coastal ecosystem and mechanistic links between sea ice and biology that are challenging to quantify solely at the regional scale.

Higher spring SIM fractions were attributed to strong northward sea-ice motion throughout the winter, consistent with previous studies, but now over a longer time seriestime series. Longer sea-ice season duration and later retreat were associated with greater water column stratification strength, not through SIM inputs but likely through the insulative effect from wind-driven mixing. Additionally, higher sea-ice persistence and stratification strength had a positive impact on depth-integrated chl-*a*. Nonetheless, sea-ice behavior alone does not fully explain the increases in stratification and in chl-*a*. Concurrently, however, there has been an increase in meteoric meltwater inputs to this area due to increases in precipitation and glacial melt in response to ongoing regional warming. Therefore, we hypothesize that the positive trends in stratification and chl-*a* are driven in part by increased meteoric meltwater inputs.

The coastal marine ecosystem is influenced by both local-scale processes and nonlocal influences that imprint on the ocean environment. Satellite-derived sea-ice concentration and motion data provide insights into regional sea-ice behavior and allow us to better understand the complex ways sea ice impacts coastal biology. While both local and nonlocal parameters continue to have limitations, this study provides insights into how a multi-scaled approach can be used to build a more complete understanding of sea-ice behavior and its effect on the coastal marine ecosystem.

Data Availability Statement

Data used here are all publicly available, primarily via the Palmer LTER Environmental Data Initiative data portal (Stable isotope data (v1): https://doi.org/10.6073/pasta/251000bc5fdcc5f11ad975295dd38774 (Meredith et al., 2021); Meteorological data including in situ sea-ice record (v8): https://doi.org/10.6073/pasta/cddd3985350334b876cd7d6d1a5bc7bf (Palmer et al., 2019); Station Chlorophyll-*a* data and Station CTD casts (v1): https://doi.org/10.6073/pasta/7358be99bd7ec1c73293893defb289d3 (Palmer et al., 2022). The Nimbus-7 SMMR and DMSP SSM/I-SSMIS satellite sea-ice concentration data (v2) are available through the National Snow and Ice Data Center (NSIDC), University of Colorado Boulder (https://doi.org/10.5067/MPYG15WAA4WX, DiGirolamo et al., 2022). Polar Pathfinder Daily 25 km sea-ice motion vectors (v4) are available through the NSIDC (https://doi.org/10.5067/INAWUWO7QH7B, Tschudi et al., 2019).

Acknowledgments
We thank all the PalLTER scientists and leaders who have contributed to this 30-year time series. We also thank Sage Lichtenwalner, Michael Cappola and Nicole Waite for processing and assisting with the PalLTER meteorological and CTD data sets. Thank you to Susannah Brodnitz and Mamadou Diawa for their contributions to data processing and analysis. Palmer LTER data were made available through the following NSF Grants OPP 9011927, 9632763, 0217282, 0823101, 1440435, 1552226, 2026045 and 2224611. E. Goodell was supported by a Student Research Assistant Grant awarded to Eveleth by Oberlin College. The participation of M. Meredith was funded by the Natural Environment Research Council via awards NE/W004933/1 (BIOPOLE) and NE/W004747/1 (DEFIANT). Geospatial support for this work provided by the Polar Geospatial Center under NSF-OPP award 1552226. We thank Sebastien Moreau and an anonymous reviewer for their thoughtful suggestions that have improved the manuscript.

References

Baba, K., Minobe, S., Kimura, N., & Wakatsuchi, M. (2006). Intraseasonal variability of sea-ice concentration in the Antarctic with particular emphasis on wind effect. *Journal of Geophysical Research*, *111*(C12), C12023. https://doi.org/10.1029/2005JC003052

Biggs, T. E. G., Alvarez-Fernandez, S., Evans, C., Mojica, K. D. A., Rozema, P. D., Venables, H. J., et al. (2019). Antarctic phytoplankton community composition and size structure: Importance of ice type and temperature as regulatory factors. *Polar Biology*, *42*(11), 1997–2015. https://doi.org/10.1007/s00300-019-02576-3

Brown, M. S., Munro, D. R., Feehan, C. J., Sweeney, C., Ducklow, H. W., & Schofield, O. M. (2019). Enhanced oceanic CO_2 uptake along the rapidly changing West Antarctic Peninsula. *Nature Climate Change*, *9*(9), 678–683. https://doi.org/10.1038/s41558-019-0552-3

Cape, M. R., Vernet, M., Pettit, E. C., Wellner, J., Truffer, M., Akie, G., et al. (2019). Circumpolar Deep Water impacts glacial meltwater export and coastal biogeochemical cycling along the West Antarctic Peninsula. *Frontiers in Marine Science*, *6*, 144. https://doi.org/10.3389/fmars.2019.00144

Carvalho, F., Kohut, J., Oliver, M. J., & Schofield, O. (2017). Defining the ecologically relevant mixed-layer depth for Antarctica's coastal seas. *Geophysical Research Letters*, *44*(1), 338–345. https://doi.org/10.1002/2016GL071205

Carvalho, F., Kohut, J., Oliver, M. J., Sherrell, R. M., & Schofield, O. (2016). Mixing and phytoplankton dynamics in a submarine canyon in the West Antarctic Peninsula. *Journal of Geophysical Research: Oceans*, *121*(7), 5069–5083. https://doi.org/10.1002/2016JC011650

Comiso, J. C., & Nishio, F. (2008). Trends in the sea ice cover using enhanced and compatible AMSR-E, SSM/I, and SMMR data. *Journal of Geophysical Research*, *113*(C2), C02S07. https://doi.org/10.1029/2007JC004257

Cook, A. J., Fox, A. J., Vaughan, D. G., & Ferrigno, J. G. (2005). Retreating Glacier fronts on the Antarctic Peninsula over the past half-century. *Science*, *308*(5721), 541–544. https://doi.org/10.1126/science.1104235

Cook, A. J., Holland, P. R., Meredith, M. P., Murray, T., Luckman, A., & Vaughan, D. G. (2016). Ocean forcing of glacier retreat in the western Antarctic Peninsula. *Science*, *353*(6296), 283–286. https://doi.org/10.1126/science.aae0017

Death, R., Wadham, J. L., Monteiro, F., Le Brocq, A. M., Tranter, M., Ridgwell, A., et al. (2014). Antarctic ice sheet fertilises the Southern Ocean. *Biogeosciences*, *11*(10), 2635–2643. https://doi.org/10.5194/bg-11-2635-2014

DiGirolamo, N., Parkinson, C. L., Cavalieri, D. J., Gloersen, P., & Zwally, H. J. (2022). Sea ice concentrations from Nimbus-7 SMMR and DMSP SSM/I-SSMIS passive microwave data, version 2 [Dataset]. *NASA National Snow and Ice Data Center Distributed Active Archive Center*. https://doi.org/10.5067/MPYG15WAA4WX

Ducklow, H. W., Baker, K., Martinson, D. G., Quetin, L. B., Ross, R. M., Smith, R. C., et al. (2007). Marine pelagic ecosystems: The west Antarctic Peninsula. *Philosophical Transactions of the Royal Society B: Biological Sciences*, *362*(1477), 67–94. https://doi.org/10.1098/rstb.2006.1955

Ducklow, H. W., Fraser, W., Meredith, M., Stammerjohn, S., Doney, S., Martinson, D., et al. (2013). West Antarctic peninsula: An ice-dependent coastal marine ecosystem in transition. *Oceanography*, *26*(3), 190–203. https://doi.org/10.5670/oceanog.2013.62

Epstein, S., & Mayeda, T. (1953). Variation of O18 content of waters from natural sources. *Geochimica et Cosmochimica Acta*, *4*(5), 213–224. https://doi.org/10.1016/0016-7037(53)90051-9

Eveleth, R., Cassar, N., Sherrell, R. M., Ducklow, H., Meredith, M. P., Venables, H. J., et al. (2017). Ice melt influence on summertime net community production along the Western Antarctic Peninsula. *Deep Sea Research Part II: Topical Studies in Oceanography*, *139*, 89–102. https://doi.org/10.1016/j.dsr2.2016.07.016

Hobbs, W. R., Massom, R., Stammerjohn, S., Reid, P., Williams, G., & Meier, W. (2016). A review of recent changes in Southern Ocean sea ice, their drivers and forcings. *Global and Planetary Change*, *143*, 228–250. https://doi.org/10.1016/j.gloplacha.2016.06.008

Hobbs, W. R., Spence, P., Meyer, A., Schroeter, S., Fraser, A. D., Reid, P., et al. (2024). Observational evidence for a regime shift in summer Antarctic sea ice. *Journal of Climate*, *37*(7), 2263–2275. https://doi.org/10.1175/JCLI-D-23-0479.1

Holland, P. R., & Kwok, R. (2012). Wind-driven trends in Antarctic sea-ice drift. *Nature Geoscience*, *5*(12), 872–875. https://doi.org/10.1038/ngeo1627

Hopwood, M. J., Carroll, D., Höfer, J., Achterberg, E. P., Meire, L., Le Moigne, F. A. C., et al. (2019). Highly variable iron content modulates iceberg-ocean fertilisation and potential carbon export. *Nature Communications*, *10*(1), 5261. https://doi.org/10.1038/s41467-019-13231-0

Kim, H., Ducklow, H. W., Abele, D., Ruiz Barlett, E. M., Buma, A. G. J., Meredith, M. P., et al. (2018). Inter-decadal variability of phytoplankton biomass along the coastal West Antarctic Peninsula. *Philosophical Transactions of the Royal Society A: Mathematical, Physical & Engineering Sciences*, *376*(2122), 20170174. https://doi.org/10.1098/rsta.2017.0174

Kimura, N. (2007). Mechanisms controlling the temporal variation of the sea ice edge in the Southern Ocean. *Journal of Oceanography*, *63*(4), 685–694. https://doi.org/10.1007/s10872-007-0060-3

Kwok, R., Comiso, J. C., Lee, T., & Holland, P. R. (2016). Linked trends in the south Pacific sea ice edge and southern oscillation index: Trends in Antarctic sea ice edge. *Geophysical Research Letters*, *43*(19), 10–295. https://doi.org/10.1002/2016GL070655

Liu, J., Zhu, Z., & Chen, D. (2023). Lowest Antarctic sea ice record broken for the second year in a row. *Ocean-Land-Atmosphere Research*, *2*, 0007. https://doi.org/10.34133/olar.0007

Lorbacher, K., Dommenget, D., Niiler, P. P., & Köhl, A. (2006). Ocean mixed layer depth: A subsurface proxy of ocean-atmosphere variability. *Journal of Geophysical Research*, *111*(C7), C07010. https://doi.org/10.1029/2003JC002157

Maksym, T. (2019). Arctic and Antarctic sea ice change: Contrasts, commonalities, and causes. *Annual Review of Marine Science*, *11*(1), 187–213. https://doi.org/10.1146/annurev-marine-010816-060610

Massom, R., Reid, P., Stammerjohn, S., Raymond, B., Fraser, A., & Ushio, S. (2013). Change and variability in East Antarctic Sea ice seasonality, 1979/80–2009/10. *PLoS One*, *8*(5), e64756. https://doi.org/10.1371/journal.pone.0064756

Meehl, G. A., Arblaster, J. M., Chung, C. T. Y., Holland, M. M., DuVivier, A., Thompson, L., et al. (2019). Sustained ocean changes contributed to sudden Antarctic sea ice retreat in late 2016. *Nature Communications*, *10*(1), 14. https://doi.org/10.1038/s41467-018-07865-9

Meier, W. N., Hovelsrud, G. K., van Oort, B. E. H., Key, J. R., Kovacs, K. M., Michel, C., et al. (2014). Arctic sea ice in transformation: A review of recent observed changes and impacts on biology and human activity: Arctic sea ice: Review of recent changes. *Reviews of Geophysics*, *52*(3), 185–217. https://doi.org/10.1002/2013RG000431

Mendes, C. R. B., Costa, R. R., Ferreira, A., Jesus, B., Tavano, V. M., Dotto, T. S., et al. (2023). Cryptophytes: An emerging algal group in the rapidly changing Antarctic Peninsula marine environments. *Global Change Biology*, *29*(7), 1791–1808. https://doi.org/10.1111/gcb.16602

Meredith, M. P., Brandon, M. A., Wallace, M. I., Clarke, A., Leng, M. J., Renfrew, I. A., et al. (2008). Variability in the freshwater balance of northern marguerite bay, Antarctic Peninsula: Results from δ18O. *Deep Sea Research Part II: Topical Studies in Oceanography*, *55*(3–4), 309–322. https://doi.org/10.1016/j.dsr2.2007.11.005

Meredith, M. P., Stammerjohn, S. E., Ducklow, H. W., Leng, M. J., Arrowsmith, C., Brearley, J. A., et al. (2021). Local- and large-scale drivers of variability in the coastal freshwater budget of the western Antarctic Peninsula. *Journal of Geophysical Research: Oceans*, *126*(6). https://doi.org/10.1029/2021JC017172

Meredith, M. P., Stammerjohn, S. E., Venables, H. J., Ducklow, H. W., Martinson, D. G., Iannuzzi, R. A., et al. (2017). Changing distributions of sea ice melt and meteoric water west of the Antarctic Peninsula. *Deep Sea Research Part II: Topical Studies in Oceanography*, *139*, 40–57. https://doi.org/10.1016/j.dsr2.2016.04.019

Meredith, M. P., Venables, H. J., Clarke, A., Ducklow, H. W., Erickson, M., Leng, M. J., et al. (2013). The freshwater system west of the Antarctic Peninsula: Spatial and temporal changes. *Journal of Climate*, *26*(5), 1669–1684. https://doi.org/10.1175/JCLI-D-12-00246.1

Moffat, C., & Meredith, M. (2018). Shelf–ocean exchange and hydrography west of the Antarctic Peninsula: A review. *Philosophical Transactions of the Royal Society A: Mathematical, Physical & Engineering Sciences*, *376*(2122), 20170164. https://doi.org/10.1098/rsta.2017.0164

Montes-Hugo, M., Doney, S. C., Ducklow, H. W., Fraser, W., Martinson, D., Stammerjohn, S. E., & Schofield, O. (2009). Recent changes in phytoplankton communities associated with rapid regional climate change along the western Antarctic Peninsula. *Science*, *323*(5920), 1470–1473. https://doi.org/10.1126/science.1164533

Nardelli, S. C., Gray, P. C., Stammerjohn, S. E., & Schofield, O. (2023). Characterizing coastal phytoplankton seasonal succession patterns on the West Antarctic Peninsula. *Limnology & Oceanography*, *68*(4), 845–861. https://doi.org/10.1002/lno.12314

Östlund, H. G., & Hut, G. (1984). Arctic Ocean water mass balance from isotope data. *Journal of Geophysical Research*, *89*(C4), 6373–6381. https://doi.org/10.1029/JC089iC04p06373

Palmer, Station Antarctica LTER, & Information Manager, P. (2019). Daily averaged weather time series (air temperature, pressure, wind speed, wind direction, precipitation, sky cover) at Palmer Station, Antarctica combining manual observations (1989 - Dec 12, 2003) and PALMOS automatic weather station measurements (Dec 13, 2003 - March 2019). (Version 8) [Dataset]. *Environmental Data Initiative*. https://doi.org/10.6073/pasta/cddd3985350334b876cd7d6d1a5bc7bf

Palmer Station Antarctica LTER, and Waite, N. (2022). Merged discrete water-column data from annual PAL LTER field seasons at Palmer Station, Antarctica, from 1991 to 2021. (Version 1) [Dataset]. *Environmental Data Initiative*. https://doi.org/10.6073/pasta/7358be99bd7ec1c73293893defb289d3

Parkinson, C. L. (2019). A 40-y record reveals gradual Antarctic sea ice increases followed by decreases at rates far exceeding the rates seen in the Arctic. *Proceedings of the National Academy of Sciences* (Vol. 116(29), 14414–14423). https://doi.org/10.1073/pnas.1906556116

Parkinson, C. L., Cavalieri, D. J., Gloersen, P., Zwally, H. J., & Comiso, J. C. (1999). Arctic sea ice extents, areas, and trends, 1978-1996. *Journal of Geophysical Research*, *104*(C9), 20837–20856. https://doi.org/10.1029/1999JC900082

Rignot, E., Mouginot, J., Scheuchl, B., van den Broeke, M., van Wessem, M. J., & Morlighem, M. (2019). Four decades of Antarctic ice sheet mass balance from 1979–2017. *Proceedings of the National Academy of Sciences* (Vol. 116(4), 1095–1103). https://doi.org/10.1073/pnas.1812883116

Rintoul, S. R. (2018). The global influence of localized dynamics in the Southern Ocean. *Nature*, *558*(7709), 209–218. https://doi.org/10.1038/s41586-018-0182-3

Saba, G. K., Fraser, W. R., Saba, V. S., Iannuzzi, R. A., Coleman, K. E., Doney, S. C., et al. (2014). Winter and spring controls on the summer food web of the coastal West Antarctic Peninsula. *Nature Communications*, *5*(1), 4318. https://doi.org/10.1038/ncomms5318

Schofield, O., Brown, M., Kohut, J., Nardelli, S., Saba, G., Waite, N., & Ducklow, H. (2018). Changes in the upper ocean mixed layer and phytoplankton productivity along the West Antarctic Peninsula. *Philosophical Transactions of the Royal Society A: Mathematical, Physical & Engineering Sciences*, *376*(2122), 20170173. https://doi.org/10.1098/rsta.2017.0173

Schofield, O., Saba, G., Coleman, K., Carvalho, F., Couto, N., Ducklow, H., et al. (2017). Decadal variability in coastal phytoplankton community composition in a changing West Antarctic Peninsula. *Deep Sea Research Part I: Oceanographic Research Papers*, *124*, 42–54. https://doi.org/10.1016/j.dsr.2017.04.014

Smith, K. L., Sherman, A. D., Shaw, T. J., Murray, A. E., Vernet, M., & Cefarelli, A. O. (2011). Carbon export associated with free-drifting icebergs in the Southern Ocean. *Deep Sea Research Part II: Topical Studies in Oceanography*, *58*(11–12), 1485–1496. https://doi.org/10.1016/j.dsr2.2010.11.027

Stammerjohn, S. E., Martinson, D. G., Smith, R. C., & Iannuzzi, R. A. (2008). Sea ice in the western Antarctic Peninsula region: Spatio-temporal variability from ecological and climate change perspectives. *Deep Sea Research Part II: Topical Studies in Oceanography*, *55*(18–19), 2041–2058. https://doi.org/10.1016/j.dsr2.2008.04.026

Stammerjohn, S. E., Martinson, D. G., Smith, R. C., Yuan, X., & Rind, D. (2008). Trends in Antarctic annual sea ice retreat and advance and their relation to El Niño–southern oscillation and southern annular Mode variability. *Journal of Geophysical Research*, *113*(C3), C03S90. https://doi.org/10.1029/2007JC004269

Stammerjohn, S. E., & Scambos, T. A. (2020). Warming reaches the South Pole. *Nature Climate Change*, *10*(8), 710–711. https://doi.org/10.1038/s41558-020-0827-8

Stroeve, J. C., Jenouvrier, S., Campbell, G. G., Barbraud, C., & Delord, K. (2016). Mapping and assessing variability in the Antarctic marginal ice zone, pack ice and coastal polynyas in two sea ice algorithms with implications onbreeding success of snow petrels. *The Cryosphere*, *10*(4), 1823–1843. https://doi.org/10.5194/tc-10-1823-2016

Tschudi, M., Meier, W. N., Stewart, J. S., Fowler, C., & Maslanik, J. (2019). Polar pathfinder daily 25 km EASE-grid sea ice motion vectors, (version 4) [Dataset]. *NASA National Snow and Ice Data Center Distributed Active Archive Center*. https://doi.org/10.5067/INAWUWO7QH7B

Tschudi, M. A., Meier, W. N., & Stewart, J. S. (2020). An enhancement to sea ice motion and age products at the National Snow and Ice Data Center (NSIDC). *The Cryosphere*, *14*(5), 1519–1536. https://doi.org/10.5194/tc-14-1519-2020

Turner, J., Barrand, N. E., Bracegirdle, T. J., Convey, P., Hodgson, D. A., Jarvis, M., et al. (2014). Antarctic climate change and the environment: An update. *Polar Record*, *50*(3), 237–259. https://doi.org/10.1017/S0032247413000296

Turner, J., Colwell, S. R., Marshall, G. J., Lachlan-Cope, T. A., Carleton, A. M., Jones, P. D., et al. (2005). Antarctic climate change during the last 50 years. *International Journal of Climatology*, *25*(3), 279–294. https://doi.org/10.1002/joc.1130

Turner, J., Dierssen, H., Schofield, O., Kim, H., Stammerjohn, S., Munro, D., & Kavanaugh, M. (2024). Changing phytoplankton phenology in the marginal ice zone west of the Antarctic Peninsula. *Marine Ecology Progress Series*, *734*, 1–21. https://doi.org/10.3354/meps14567

Turner, J., Holmes, C., Caton Harrison, T., Phillips, T., Jena, B., Reeves-Francois, T., et al. (2022). Record low Antarctic sea ice cover in February 2022. *Geophysical Research Letters*, *49*(12). https://doi.org/10.1029/2022GL098904

Turner, J., Lu, H., White, I., King, J. C., Phillips, T., Hosking, J. S., et al. (2016). Absence of 21st century warming on Antarctic Peninsula consistent with natural variability. *Nature*, *535*(7612), 411–415. https://doi.org/10.1038/nature18645

Vaughan, D. G., Marshall, G. J., Connolley, W. M., Parkinson, C., Mulvaney, R., Hodgson, D. A., et al. (2003). In *Recent rapid regional climate warming on the Antarctic Peninsula* (Vol. 32).

Venables, H. J., Clarke, A., & Meredith, M. P. (2013). Wintertime controls on summer stratification and productivity at the Western Antarctic Peninsula. *Limnology & Oceanography*, *58*(3), 1035–1047. https://doi.org/10.4319/lo.2013.58.3.1035

Venables, H. J., Meredith, M. P., Hendry, K. R., Ten Hoopen, P., Peat, H., Chapman, A., et al. (2023). Sustained year-round oceanographic measurements from Rothera research station, Antarctica, 1997–2017. *Scientific Data*, *10*(1), 265. https://doi.org/10.1038/s41597-023-02172-5

Vernet, M., Martinson, D., Iannuzzi, R., Stammerjohn, S., Kozlowski, W., Sines, K., et al. (2008). Primary production within the sea-ice zone west of the Antarctic peninsula: I—sea ice, summer mixed layer, and irradiance. *Deep Sea Research Part II: Topical Studies in Oceanography*, *55*(18–19), 2068–2085. https://doi.org/10.1016/j.dsr2.2008.05.021

Wallis, B. J., Hogg, A. E., Meredith, M. P., Close, R., Hardy, D., McMillan, M., et al. (2023). Ocean warming drives rapid dynamic activation of marine-terminating glacier on the west Antarctic Peninsula. *Nature Communications*, *14*(1), 7535. https://doi.org/10.1038/s41467-023-42970-4

World Meteorological Organization. (2017). *Manual on codes volume I.2 annex II to the WMO technical regulations Part B- binary codes Part C-common features to binary and alphanumeric codes, 2019 edition, updated in 2022*. WMO. Retrieved from https://library.wmo.int/idurl/4/35625.1238pp.

Wouters, B., Martin-Español, A., Helm, V., Flament, T., van Wessem, J. M., Ligtenberg, S. R. M., et al. (2015). Dynamic thinning of glaciers on the southern Antarctic peninsula. *Science*, *348*(6237), 899–903. https://doi.org/10.1126/science.aaa5727